Quantum Monte-Carlo simulations of two-component Bose mixtures

Cikojević, Viktor

Master's thesis / Diplomski rad

2016

Degree Grantor / Ustanova koja je dodijelila akademski / stručni stupanj: **University of Split, University of Split, Faculty of science / Sveučilište u Splitu, Prirodoslovno-matematički fakultet**

Permanent link / Trajna poveznica: https://urn.nsk.hr/urn:nbn:hr:166:816711

Download date / Datum preuzimanja: **2025-03-29**

Repository / Repozitorij:

Repository of Faculty of Science

Quantum Monte Carlo simulations of two-component Bose mixtures

Viktor Cikojević

Supervisors: prof. dr. sc. Leandra Vranješ-Markić
prof. dr. sc. Jordi Boronat

Split, September 2016

MASTER THESIS

Contents

Chapter 1

Introduction

Experimental realization of Bose-Einstein codensation [2] opened the door
to now one of the most active subfields of condensed matter physics, physics
of ultracold systems. The main obstacle in realizing the Bose-Einstein con-
densation is achieving cold enough temperatures in which the Bose-Einstein
phase occurs. For example, in a vapour of rubidium-87 atoms, experimental
group from paper [2] had to achieve the temperature of the sample below 170
nK. Nowadays, in the laboratories the degenerate Bose and Fermi gases of
single and two component alkali metals are produced routinely, and recently
two component systems started to get more theoretical and experimental ac-
tivities. They have been used to investigate different phenomena related to
the research of interacting quantum systems. Two components mean either
the same atoms in different hyperfine states or just two different atoms.

Two main features that are accessible to experimental ultracold physics
are [3] i) control of the interparticle interaction using the phenomena of
Fesbach resonances and ii) precise manipulation of external traps with the
ability to change the dimensionality, shape and the strength of potentials
using lasers or external magnetic fields.

Because the systems are at ultracold temperatures, de Broglie wavelength
of the atoms in the trap is much bigger than the range of interaction, so
the atom collisions are mostly isotropic s-wave scatterings. Therefore, the
interaction can be described using one parameter only: the s-wave scattering
length a. Besides the fact that this greatly simplifies the description of the
interaction, it is interesting that the s-wave scattering length can be tuned
with external magnetic field using the phenomena of Fesbach resonance, with

the relation between a and B usually taken as

$$a(B) = a_0 \left(1 - \frac{\Delta B}{B - B_0} \right) \qquad (1.1)$$

Theoretical description of ultracold systems is usually made by solving the Gross-Pitaevski equation, a mean field approximation of the system. In other words, the potential that each atom experiences is approximated to be the averaged effect of the rest $N - 1$ atoms in the system. This approximation usually gives very good results primarily because the systems under consideration are very dilute, in the order of 10^{12}-10^{14} atoms$/cm^3$[2]. Relevant parameter that we assocciate with the applicability of diluteness approximation is the gas parameter na^3, which arises as the perturbation parameter when calculating the ground state energy with the perturbation theory of homogenous Bose systems (Eq. 1.2). In the limit na^3 the mean field approximation, the first term in Eq. (1.2), becomes exact. Quantum Monte Carlo calculations [5] show agreement between the perturbation theory and numerical results.

$$E/N = 4\pi na^3 \times \left[1 + \frac{128}{15\sqrt{\pi}}\sqrt{na^3} + \frac{8(4\pi - 3\sqrt{3})}{3}na^3 \ln(na^3) + ... \right] \qquad (1.2)$$

In the case of two-component systems with repulsive interactions in a trap, the first thing to understand is the criteria of miscibility of two species. In the case of homogenous Bose-Bose gases, the miscibility criteria follows from the interaction term $\sum_{ij} g_{ij}n_i n_j$, that must be positive definite and so the miscibility criteria is $g_{12}^2 < g_{11}g_{22}$. These systems are usually trapped in a harmonic trap which plays the stabilizing role, so the question is how the miscibility criteria changes due to the trapping. In the Thomas-Fermi limit Na/a_{ho}, where N is the number of particles and a is the scattering length, system in the trap behaves locally as a homogenous gas [23], but still we do not have a complete picture outside the Thomas-Fermi limit for the two-component systems. It is clear that for the very weak interaction the density profiles will not not so different from the ideal gas profiles, due to the stabilizing role of the trap, and it is interesting to ask for which strength of interaction the phenomena of separation will occur.

Another interesting problem appears in the systems with attractive interaction between atoms of different species. In the case of homogenous Bose-Bose gas, the criteria of stability is again $g_{12}^2 < g_{11}g_{22}$. When this criteria is

3

not fulfiled, the solutions to the Gross-Pitaevski equation do not exist, and the system collapses. The prediction in [7] says that in the regime unstable viewed from the mean field thory, there is a droplet that has a very weakly bound state. If experimentally realised, this could be liquid with the lowest density ever observed. Mechanism of stabilization of the droplet comes from attractive mean field term which scales as $\sim n^2$, and a repulsive beyond mean field term that scales with $\sim n^{5/2}$. The phenomena of droplet formation is already confirmed in 1D and 2D geometries [8] using quantum Monte Carlo methods. In lower dimensions this phenomena of droplet formation is more pronounced since there is always a two-particle bound state for $a < 0$ in 1D and 2D, which is not a case in 3D.

Using the quantum Monte Carlo methods, Variational Monte Carlo and Diffusion Monte Carlo combined, we can determine the ground state properties of many-particle systems exactly, within the statistical uncertainties. This is why we used Monte Carlo to investigate two-component Bose systems.

1.1   Outline of the thesis

In Chapter (2) we concetrate on the theoretical results from quantum mechanics that are most relevant for this thesis. We start by discussing general two-atom scattering in a vacuum, which is the dominant effect in the many-body dilute systems. Then we derive the long-range behaviour of such scattering, where it is shown that complete effect of the interaction can be encoded in a single number: the scattering length a. We write the relations between parameters of interaction and the scattering length for the simple potentials that were used in our calculations. Finally, we derive Gross-Pitaevski equation for the many-body Bose system.

In Chapter (3) the numerical methods used in the thesis are presented. We implemented both Variational Monte Carlo (VMC) and Diffusion Monte Carlo(DMC) methods in C++ programming language. These methods combined are used to solve many-body Schroedinger equation at zero temperature exactly.

In Chapter (4) the properties of two-component repulsive Bose gase in harmonic trap are presented. First we made test runs of our code, and found the range of applicability of using scattering length for describing the interactions solely, for the systems containing at most 100 particles. Then we investigated the phase diagram as defined in [12], to compare our results the

the predictions of the mean field theory. For the same points in the phase diagram as in [12], our calculations show some deviations and an indication that the phase diagram must be spanned differently to account for the mass disbalance and the interaction strength.

In Chapter (5) we present results of the Bose mixture with repulsive interspecies and attractive intraspecies interaction. First we made test runs of the code, and then we determine the properties of the weakly bound droplet on a variational level, in an unstable regime viewed from the mean field point, for the systems containing at most 200 particles. Our calculations show that for the model used, in order to describe the droplet formation scattering length is not the only relevant parameter.

Chapter 2

Theoretical background

Underlying microscopic theory of ultracold Bose gases is quantum mechanics. In position representation of a quantum mechanical state, the wavefunction $\psi(\boldsymbol{r})$ of N non-relativistic spinless particles interacting with the pair potential V_{int}, subject to the external potential V_{ext}, is governed by the Schroedinger equation [21]

$$i\hbar\frac{\partial\psi(\boldsymbol{R},t)}{\partial t} = \hat{H}\psi(\boldsymbol{R},t) \qquad (2.1)$$

where the Hamiltonian is given by

$$\hat{H} = -\sum_{i=1}^{n}\frac{\hbar^2\nabla_i^2}{2m} + \sum_{i=1}^{n}V_{ext}(\boldsymbol{r}_i) + \sum_{i=1}^{n}\sum_{j=i+1}^{n}V_{int}(|\boldsymbol{r}_i - \boldsymbol{r}_j|) \qquad (2.2)$$

Wavefunction ψ from (2.1) contains all the information about the system. Physical quantities that are measured experimentally are the eigenvalues of some linear Hermitian operator. It is usually very hard to find solutions of (2.1) for most many-body problems, if not impossible. Therefore, usual theoretical description of many-body ultracold systems involve approximations, such as the mean-field theory.

In this chapter we present theoretical background needed for the description of two-component ultracold Bose gases. We will start by discussing the two-atom scattering in vacuum (Sec. 2.1), where we introduce the crucial parameter for describing the interaction: the scattering length a. In simulating many-body systems we use trial wavefunctions as an input for the algorithms (Ch. 3), written as a product of two-particle correlation functions, so we write down the analytical solutions of the two-body problem

for the potentials we use in Sec. 2.2. Finally, we conclude the chapter by deriving the Gross-Pitaevski equation, which is a mean field description of many-body ultracold Bose systems (Sec. 2.3).

2.1   Two-atom scattering solution

Let us consider scattering of two spinless nonrelativistic atoms in vacuum, interacting with isotropic potentials, without the external potentials. We are interested in low-energy physics of such processes, since the experiments in ultracold gases are made in that limit. The complete description of the system is given by the Schroedinger equation (2.1)

$$\left\{ \frac{-\hbar^2 \nabla_1^2}{2m_1} + \frac{-\hbar^2 \nabla_2^2}{2m_2} + V_{int}(\boldsymbol{r}_1, \boldsymbol{r}_2) \right\} \psi(\boldsymbol{r}_1, \boldsymbol{r}_2) = E\psi(\boldsymbol{r}_1, \boldsymbol{r}_2) \qquad (2.3)$$

The problem (2.3) is reduced to one-body problem after making a transformation to $\boldsymbol{r} = \boldsymbol{r}_1 - \boldsymbol{r}_2$, $\boldsymbol{r}_{CM} = \sum_i m_i \boldsymbol{r}_i/(m_1 + m_2)$. In the new basis, the wave function automatically satisfyes Bose statistics, since $\psi(\boldsymbol{r}) = \psi(r)$ for isotropic potentials, and the solution can be written as $\psi(\boldsymbol{r}_1, \boldsymbol{r}_2) = \psi_{cm}(\boldsymbol{r}_{CM})\psi(\boldsymbol{r})$. The Eq. (2.3) then decouples to two equations, one for center of mass, and the other for fictitous particle of mass $\mu = m_1 m_2/(m_1 + m_2)$ given by

$$\left\{ \frac{-\hbar^2 \nabla^2}{2\mu} + V_{int}(\boldsymbol{r}) \right\} \psi_{rel}(\boldsymbol{r}) = E\psi_{rel}(\boldsymbol{r}) \qquad (2.4)$$

The solution for center of mass wavefunction are trivial plane waves, so the physics is essentially determined by ψ_{rel}, which will be denoted as ψ from now on. Another way of writing the Eq. (2.4) is

$$\left\{ \nabla^2 + k^2 \right\} \psi(\boldsymbol{r}) = V_{int}(\boldsymbol{r})\psi(\boldsymbol{r}) \qquad (2.5)$$

where $k^2 = 2\mu E/\hbar^2$. The wavefunction is formally written as a superposition of homogenous and particular solutions of (2.5)

$$\psi(\boldsymbol{r}) = \psi(\boldsymbol{r})_{homo} - \frac{\mu}{2\pi\hbar^2} \int d^3 r' \frac{\exp\left(ik \left| \boldsymbol{r} - \boldsymbol{r}' \right|\right)}{\left| \boldsymbol{r} - \boldsymbol{r}' \right|} V(\boldsymbol{r}')\psi(\boldsymbol{r}') \qquad (2.6)$$

ψ is not yet determined since it appears on both left and right hand side of Eq. (2.6). However we can get the solution using approximation $\left| \boldsymbol{r} - \boldsymbol{r}' \right| \gg 0$,

7

for all $\boldsymbol{r}'$. This is justified by the fact that the mean interparticle distance in ultracold experiments is much larger than the range of potential. In the regions where the potential is significant, the wavefunction is negligible and vice versa. This simplyfies the expression of the particular solution, using the limits

$$k \left|\boldsymbol{r} - \boldsymbol{r}'\right| \xrightarrow[r \to \infty]{} kr - \boldsymbol{k}\frac{\boldsymbol{r}}{r}r' \tag{2.7}$$

$$\frac{1}{\left|\boldsymbol{r} - \boldsymbol{r}'\right|} \xrightarrow[r \to \infty]{} \frac{1}{r} \tag{2.8}$$

with the definition of $\boldsymbol{k}' = k\boldsymbol{r}/r$, the wave vector of the scattered state. The solution of [?] is given with

$$\psi(\boldsymbol{r}) = A \left\{ \exp(i\boldsymbol{k}\boldsymbol{r}) - \frac{\exp(ikr)}{r} \frac{\mu}{2\pi\hbar^2} \int d^3r \exp(-i\boldsymbol{k}'\boldsymbol{r}')V(\boldsymbol{r}')\psi(\boldsymbol{r}') \right\} \tag{2.9}$$

We are interested only in the first order effect of the potential to the incoming wave with wavevector $\boldsymbol{k}$. This is known as Born approximation, and it is valid for $r \gg 0$, since the Born series give expansions in terms of $1/r^n$. Putting the $\exp(i\boldsymbol{k}\boldsymbol{r})$ into the integrand in Eq. (2.9) we get

$$\psi(\boldsymbol{r}) = A \left\{ \exp(i\boldsymbol{k}\boldsymbol{r}) + f(\boldsymbol{k}', \boldsymbol{k})\frac{\exp(ikr)}{r} \right\} \tag{2.10}$$

$$f(\boldsymbol{k}', \boldsymbol{k}) = -\frac{\mu}{2\pi\hbar^2} \int d^3r \exp(-i\left[\boldsymbol{k}' - \boldsymbol{k}\right]\boldsymbol{r}')V(\boldsymbol{r}') \tag{2.11}$$

The quantity $f(\boldsymbol{k}', \boldsymbol{k})$ is called the scattering amplitude. Eq. (2.10) is understood in the following way. Total wavefunction is a superposition of the incoming plane wave with wavevector $\boldsymbol{k}$ and an outgoing spherical wave with the wavevector $\boldsymbol{k}'$. The role of interaction is to change a state from $|\boldsymbol{k}\rangle$ to $|\boldsymbol{k}'\rangle$, as presented in the Fig. 2.1.
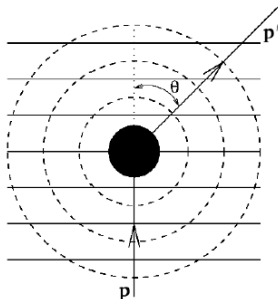
Figure 2.1: Schematic representation of interaction. Incoming plane wave of momentum $\boldsymbol{p}$, presented with solid lines, scatters into the spherical wave, denoted by dashed lines, with momentum $\boldsymbol{p}'$. Figure adapted from [22]

We see from Eq. (2.11) that the complete interaction is determined by scattering amplitude $f(\boldsymbol{k}', \boldsymbol{k})$. It is now shown how the description can be simplified in the low-energy limit, or in other words when $k \approx 0$. For $\boldsymbol{k}' = \boldsymbol{k} = 0$, the scattering amplitude is

$$f(0,0) = -\frac{\mu}{2\pi\hbar^2} \int d^3 r V(\boldsymbol{r}') \tag{2.12}$$

It is then convinient to use effective potential in the low-energy limit that reproduces the scattering amplitude. For $\boldsymbol{k} \neq 0$, since the interaction is isotropic, we can expand the incoming wave as a sum of angular momentum eigenstates

$$\exp(i\boldsymbol{k}\boldsymbol{r}) = \sum_{l=0}^{\infty} i^l (2l + 1) j_l(kr) P_l(\cos(\theta)) \tag{2.13}$$

where $j_l(kr)$ are spherical Bessel functions. Under the assumption of large interparticle distances, we use the large r limit of Bessel functions

$$j_l(kr) \xrightarrow[r\to\infty]{} \frac{\sin(kr - l\pi/2)}{kr} \tag{2.14}$$

We limit ourselves to elastic scattering, so the $f(\boldsymbol{k}', \boldsymbol{k})$ is actually a function of k and angle θ between $\boldsymbol{k}$ and $\boldsymbol{k}'$. This allows us to expand the scattering amplitude as a sum of angular momentum eigenstates as well

$$f(\boldsymbol{k}', \boldsymbol{k}) = \sum_{l=0}^{\infty} (2l + 1) f_l(k) P_l(\cos(\theta)) \tag{2.15}$$

9

where P_l are Legendre polynomials of order l, and $f_l(k)$ are to be determined. Putting the Eqs. (2.13) and (2.15) into Eq. (2.10) we get

$$\psi = A \sum_{l=0}^{\infty} (2l+1) P_l(\cos(\theta)) \left[\frac{\exp(-ikr + il\pi)}{2ikr} + \frac{\exp(ikr)}{r} \left(f_l(k) + \frac{1}{2ik} \right) \right]$$

(2.16)

In the absence of the interaction $f_l(k) = 0$, and the solution is given by the sum of incoming and outgoing spherical waves with definite angular momentum. With the interaction turned on, the complex coeficients multiplying outgoing spherical components change. In other words, turning the interaction can be seen as an unitary transformation which changes the phase of each angular momentum eigenstate. This defines the phase shifts $\delta_l(k)$ as

$$\exp(2i\delta_l(k)) = 1 + 2ik f_l(k)$$

(2.17)

In the experiments with ultracold atoms, the energy of each atom is much smaller than the centrifugal barrier $\sim l(l+1)/r^2$ arising from particles being in different angular momentum eigenstates. Therefore it is a good approximation to say that only $l = 0$ state is affected by the interaction. For the two-atom problem in this aproximation the scattering amplitude is written as

$$f(\boldsymbol{k}, \boldsymbol{k}') = f_0(k) = \frac{\exp(2i\delta_0(k)) - 1}{2ik} = \frac{1}{k \cot(\delta_0(k)) - ik}$$

(2.18)

In the low-energy scattering approximation it is useful to define the scattering length a as

$$a = -\lim_{k \to 0} \frac{\delta_0(k)}{k}$$

(2.19)

because we can relate the scattering length with the scattering amplitude of zeroth partial wave

$$\lim_{k \to 0} f_0(k) = -a$$

(2.20)

where we used the expansion [22]

$$k \cot [\delta_0(k)] = -\frac{1}{a} + \frac{1}{2} r_{\text{eff}} k^2 + \dots$$

(2.21)

The parameter r_{eff} in the expansion (2.21) is called the effective range of the potential, which needs to be taken into account for more precise determination of system properties. This term is usually omitted when studying

ultracold atoms since both k and r_{eff} are very small, which makes the first term in Eq. (2.21) the most relevant one. Therefore, the effect of two-body interaction is encoded in a single parameter, the scattering length a. This is an important result that is later used for solving the many-body problem. Since the scattering length can be controlled using external magnetic field, it allows us to study systems *ab initio* with the control of interaction. This is also the reason why numerical studies of ultracold systems can give the exact description of bosonic system, since it is sufficient to use any potential that reproduces wanted scattering length. In the next section 2.2 we construct repulsive and attractive interaction which we will use for numerical studies.

But before proceding to construction of potentials with a given a, we will discuss what is the physical meaning of scattering length. For $k \to 0$ the exponential factors in Eq. (2.10) can be considered very small. Then the wavefunction will have the following asymptotic form

$$\psi \sim 1 - \frac{a}{r} \tag{2.22}$$

Wavefunction (2.22) is plotted in Figure 2.2, where we see two different long-range behaviours that depend on the sign of a. For $a > 0$ the particles prefer to be far apart, which is described as an effective repulsive interaction, whereas for $a < 0$ the particles feel effective attractive interaction.
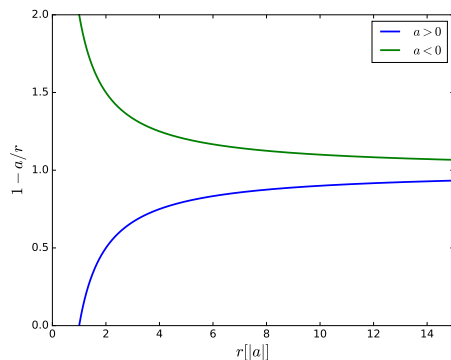

Figure 2.2: Asymptotic wavefunction for different values of scattering length a. The tendency of a wavefunction to go out or to the region of interaction is what gives the physical picture for the scattering length. Positive (negative) scattering length means there is an effective repulsive (attractive) interaction between the particles.

2.2 Models of interaction

In our analysis of two component bosonic mixture we consider dilute systems that interact both repulsively and attractivly. In this sections we construct simple potentials that reproduce wanted scattering length. We model repulsive interaction with hard-sphere potential, and attractive one with the square-well potential. Solution to the two-boy problem is also given, which will be used to construct the trial wave function of the many-body system.

Both the hard-sphere and attractive square well potentials can be written as

$$V_{sq}(r) = \begin{cases} V_0 & r < R \\ 0 & r > R \end{cases} \tag{2.23}$$

where r is the distance between the two particles. It suffices to find the solution to the two-body problem for the relative wavefunction

$$\left\{ -\frac{\hbar^2 \nabla^2}{2\mu} + V_{sq}(r) \right\} \psi(r) = E\psi(r) \tag{2.24}$$

Since $V_{sq}(r)$ is isotropic, the general solution in the form $\psi = R_{nl}(r)Y_{lm}(\theta, \phi)$. However, we are interested only in the $l = 0$ solution, so the wavefunction is $\psi = u(r)/r$, and $u(r)$ satisfies

$$\left\{ \frac{d^2}{dr^2} + k^2 - \frac{2\mu V_{sq}(r)}{\hbar^2} \right\} u(r) = 0 \tag{2.25}$$

where $k^2 = 2\mu E/\hbar^2$. The solution to Eq. (2.25) is given by

$$u(r) = \begin{cases} A\left(\exp(i\kappa r) - \exp(-i\kappa r)\right) & r < R \\ C\exp(ikr) + D\exp(-ikr) & r > R \end{cases} \tag{2.26}$$

where $\kappa^2 = k^2 - 2\mu V_0/\hbar^2$. We are interested in the asymptotic solution, which is most relevant for the ultracold systems. The $r \to \infty$ limit of $u(r)$ behaves as a Bessel function

$$\lim_{r \to \infty} u(r) = \frac{C_0}{k} \sin(kr + \delta_0) \tag{2.27}$$

$$= \frac{C_0}{k} \exp(-i\delta_0) \left[\exp(ikr) \exp(2i\delta_0) - \exp(-ikr) \right] \tag{2.28}$$

Dropping the numerical prefactors which are just normalization conditions, we see that the solution is given by

$$u(r) = \begin{cases} \exp(i\kappa r) - \exp(-i\kappa r) & r < R \\ \exp(-ikr) - \exp(ikr)\exp(2i\delta_0) & r > R \end{cases} \quad (2.29)$$

The only constant left undetermined is δ_0. Requiring for the solutions $u(R^-) = u(R^+)$ and $du/dr(R^-) = du/dr(R^+)$ we get

$$\delta_0(k) = -kR + \arctan\left[\frac{k}{\kappa}\tan(\kappa R)\right] \quad (2.30)$$

2.2.1 Effective repulsive interaction

Taking the $V_0 \to \infty$ limit of Eq. (2.30) we get

$$\delta_0(k) = -kR \quad (2.31)$$

Comparing the result (2.31) with the definition of the scattering length (Eq. 2.19), we see that the hard-sphere radius coincides with the scattering length. Therefore, the effective repulsive interaction with the given scattering length $a > 0$ can be modeled as a hard-sphere potential

$$V(r) = \begin{cases} \infty & r < a \\ 0 & r > a \end{cases} \quad (2.32)$$

in the low-energy limit.

2.2.2 Effective attractive interaction

Taking $-\infty < V_0 < 0$, from Eq. (2.30) we get

$$a = R\left(1 - \frac{\tan\gamma}{\gamma}\right) \quad (2.33)$$

$$\gamma = R\sqrt{\frac{2\mu|V_0|}{\hbar^2}} \quad (2.34)$$

In the low-energy limit whenever the square well potential supports new bound state, the scattering length diverges. This turns out to be a general property of interaction [22], but it will not be proven in this thesis.

2.3 Mean field theory of Bose systems

The aim of this thesis is to investigate properties of dilute many-body Bose gases. In this section the mainstream theoretical framework of such system is presented: the mean-field theory. [4].

The general Hamiltonian of Bose systems can be written in second quantisation formalism

$$\hat{H} = \int d^3 r \hat{\psi}^\dagger(\boldsymbol{r}) \left[-\frac{\hbar^2 \nabla^2}{2m} + \hat{V}_{ext}(\boldsymbol{r}) \right] \hat{\psi}(\boldsymbol{r}) +$$
$$\frac{1}{2} \int d^3 r d^3 r' \hat{\psi}^\dagger(\boldsymbol{r}) \hat{\psi}^{\dagger\prime}(\boldsymbol{r'}) \hat{V}(\boldsymbol{r} - \boldsymbol{r'}) \hat{\psi}(\boldsymbol{r}) \hat{\psi}'(\boldsymbol{r'}) \tag{2.35}$$

where the field operator is $\hat{\psi}^\dagger = \sum_i \varphi_i a_i^\dagger$, φ_i being the single-particle state i, and $a_i^\dagger$ is creation operator satisfying Bose commutation relation

$$\left[\hat{a}_i, \hat{a}_j^{\ \dagger} \right] = \delta_{ij} \tag{2.36}$$
$$\left[\hat{a}_i, \hat{a}_j \right] = 0 \tag{2.37}$$

The equation of motion for $\hat{\psi}$ is given by

$$i\hbar \frac{\partial}{\partial t} \hat{\psi} = \left[\hat{\psi}, \hat{H} \right] \tag{2.38}$$
$$= \left\{ -\frac{\hbar^2 \nabla^2}{2m} + V_{ext}(\boldsymbol{r}) + \int d^3 r \hat{\psi}^\dagger \hat{V}(\boldsymbol{r} - \boldsymbol{r'}) \hat{\psi} \right\} \hat{\psi} \tag{2.39}$$

At ultracold temperatures, system occupyes the low energy part of the spectrum, and there is a macroscopic number of particles in the ground state φ_0. Mean field theory is a supstitution of $\hat{a}_0$ operator with its expectation value, a complex number, which is proportional to $\sqrt{N_0}$, where N_0 is the number of particles in the ground state. In that approximation the field operator obtains the form

$$\hat{\psi} = \psi_0 + \delta\hat{\psi} \tag{2.40}$$

In other words, low energy limit of the quantum field ψ is a classical field ψ_0, which we call the condensate wavefunction, and $\delta\hat{\psi}$ is the noncondensed component of $\hat{\psi}$. In order to make supstition $\hat{\psi} \rightarrow \psi_0$ in the Eq. 2.39, we must also replace $V(\boldsymbol{r} - \boldsymbol{r'})$ with the effective potential that reproduces

the samo low-energy part of the spectrum. The easiest potential to handle analyticaly is point interaction

$$V(\boldsymbol{r} - \boldsymbol{r}') = \frac{4\pi\hbar^2 a}{m}\delta(\boldsymbol{r} - \boldsymbol{r}') \qquad (2.41)$$

This potential is chosen so that it reproduces wanted scattering length a, which can be seen from Eq. (2.12) and (2.20). Putting the potential (2.41) into (2.39), in the low-energy limit we obtain so called Gross-Pitaevski equation

$$-i\hbar\frac{\partial}{\partial t}\psi_0 = \left\{-\frac{\hbar^2\nabla^2}{2m} + V_{ext}(\boldsymbol{r}) + \frac{4\pi\hbar^2(N-1)a}{m}\left|\psi_0(\boldsymbol{r})\right|^2\right\}\psi_0(\boldsymbol{r}) \quad (2.42)$$

To obtain the time-independent Gross-Pitaevski equation, we first notice that for big N the states $|N\rangle$ and $|N+1\rangle$ are indistinguashble, so the condensate wave function is $\psi_0(\boldsymbol{r}, t) = \left\langle \hat{\psi}(\boldsymbol{r}, t) \right\rangle = \langle N | \hat{\psi}(t) | N+1 \rangle = \exp(-i\mu t/\hbar)\psi_0(\boldsymbol{r})$, since $|N(t)\rangle = \exp(-iE(n)t/\hbar)|N\rangle$ and $\mu = \partial E/\partial N \approx E(N+1) - E(N)$. Then the equation becomes

$$\left\{-\frac{\hbar^2\nabla^2}{2m} + V_{ext}(\boldsymbol{r}) + \frac{4\pi\hbar^2(N-1)a}{m}\left|\psi_0(\boldsymbol{r})\right|^2 - \mu\right\}\psi_0(\boldsymbol{r}) = 0 \qquad (2.43)$$

The Gross-Pitaevski equation is equivalent to the Hartree-Fock approximation, which can be seen by minimizing $\langle\psi_H| \hat{H}_{\text{eff}} |\psi_H\rangle$ for a system wavefunction

$$\psi_H(\boldsymbol{r}_1, \boldsymbol{r}_2, ..., \boldsymbol{r}_N) = \prod_{i=0}^{N}\varphi(\boldsymbol{r}_i) \qquad (2.44)$$

where $\varphi(\boldsymbol{r}_i)$ is single particle wavefunction and $\hat{H}_{\text{eff}}$ is the effective Hamiltonian

$$\hat{H}_{\text{eff}} = -\sum_{i=0}^{N}\frac{\hbar^2\nabla_i^2}{2m} + \sum_{i<j}\frac{4\pi\hbar^2 a}{m}\delta(\boldsymbol{r}_i - \boldsymbol{r}_j) \qquad (2.45)$$

The most serious drawback of the Gross-Pitaevski is that it does not include correlations among particles. Since correlations are suppresed in the low density regime, the GP equation can predict a number of properties. However, the main goal of this thesis is to investigate physics beyond mean field regime. The main criteria that we test in our calculations is the stability of two species condensate, which is obtained only when $g_{12}^2 < g_{11}g_{22}$. This stability requirement comes from imposing the interaction term $\sum g_{ij}n_in_j$ to be positive definite.

15

Chapter 3

Numerical Methods

In this chapter numerical algorithms used to simulate bosonic systems are presented. The acceptance-rejection Metropolis algorithm is used to calculate integrals in multidimensional Hilbert space (Sec. 3.1). Data grouping is used to estimate the standard deviation correctly, since two consecutive steps in simulation are generally correlated (Sec. 3.2). Variational Monte Carlo (Sec. 3.3) and Diffusion Monte Carlo (Sec. 3.4) methods, which are used combined to determine properties of the ground state of the system are also covered.

3.1   Metropolis algorithm

Metropolis algorithm is a method of sampling random events according to the given distribution function. In Monte Carlo simulation presented in this thesis the algorithm will be used to evaluate integrals that have the following form

$$\int d\boldsymbol{R}\, f(\boldsymbol{R})\rho(\boldsymbol{R}) \tag{3.1}$$

This integral can be reduced to the sum

$$\int d\boldsymbol{R}\, f(\boldsymbol{R})\rho(\boldsymbol{R}) = \lim_{N\to\infty} \frac{1}{N}\sum_{i=1}^{N} f(\boldsymbol{R}_i) \tag{3.2}$$

where the $\boldsymbol{R}_i$ are randomly generated n-dimensional vectors, drawn from the given distribution $\rho(\boldsymbol{R})$. The sum in eq. 3.2 for finite N is obtained by introducing the concept of *walkers*. A walker is a point in phase space $\Omega \subseteq \mathbb{R}^n$ of our system. The name walker comes from the fact that at each time step,

the walker changes its position in Ω randomly, following the distribution ρ. The rate of exploring the phase space is determined by the *step size* of walker. The more walkers we have, the better the statistics, and the equation (3.2) for N_w walkers is

$$\int d\mathbf{R}\, f(\mathbf{R})\rho(\mathbf{R}) = \sum_{i=1}^{N_w} \frac{1}{N_w} \left(\sum_{i=1}^{N_{\text{steps}}} \frac{1}{N_{\text{steps}}} f(\mathbf{R}_{i;iw}) \right) \tag{3.3}$$

where N_{steps} is number of steps for each walker. Metropolis algorithm is given below:

1. Generate random step $\Delta\mathbf{R}$

2. Calculate transition probability $T = \frac{\rho(\mathbf{R}+step\times\Delta\mathbf{R})}{\rho(\mathbf{R})}$

3. if $T \geq 1$ the step 2 is accepted, and we proceed to 5

4. if $T < 1$ the step is accepted only if $r \leq T$, where r is random number in interval $[0, 1]$. If accepted, proceed to 5

5. Calculate $f(\mathbf{R}_{new})$, where $\mathbf{R}_{new} = \mathbf{R} + \Delta\mathbf{R}$ is the new position of the walker

6. Update the size of the step: if the acceptance rate is greater (less) than the wanted acceptance rate, then decrease (increase) the step size

Metropolis algorithm is used both to reach equilibrium distribution and to sample over phase space of our system. This statistical process is called Markov process, for which two different space points $\mathbf{R}$ and $\mathbf{R}'$ are related by

$$\rho(\mathbf{R})T(\mathbf{R} \to \mathbf{R}') = \rho(\mathbf{R}')T(\mathbf{R}' \to \mathbf{R}) \tag{3.4}$$

The relation (3.4) is called detailed balance and it is the most important premise of Metropolis algorithm. Eq. (3.4) is fulfilled in equilibrium, so imposing this in the algorithm makes the system reach equilibrium asymptotically. It is very important to note that the size of a step is a variable during simulation. In most problems, the optimal percentage of accepted steps is taken to be in the interval $30\% - 50\%$ to ensure that the the walker moves through the phase space as quickly as possible.

The only problem left with calculating the integral with Metropolis algorithm approach is correlation between two successive steps. Therefore the binning of data, presented in section 3.2, needs to be done to ensure that the deviation is correctly calculated.

3.2 Data analysis

Measure of uncertainty in calculating the integral in eq. (3.2) must be treated carefully because two successive steps of walkers are generally correlated. For uncorrelated samples, the measure of uncertainty is determined from standard deviation, given by

$$\sigma = \sqrt{\frac{1}{n} \sum_i^n (f_i - \langle f \rangle)^2} \xrightarrow[n \gg 1]{} \sqrt{\langle f^2 \rangle - \langle f \rangle^2} \tag{3.5}$$

where n is the total number of data of a given function f. The main question is how much steps we must take per block to safely say that two consecutive blocks have very low correlation. The solution is to divide data into blocks, calculate averages of f in each block and then take these averages to be uncorrelated samples for sufficiently big block sizes.

Let n_s be the number of steps in each block, and n_b be the number of data blocks per simulation. The correct way to calculate the standard deviation is then given by

$$\sigma_{n_b}^2 = \frac{1}{n_b - 1} \sum_i^{n_b} \left[\langle f^2 \rangle_i - \langle f \rangle^2 \right] \tag{3.6}$$

where $\langle f^2 \rangle_i$ is the average of f^2 in the ith block, and $\langle f \rangle$ is average over all samples. Usual procedure in simulations is done in the following way. During the simulation the value of f is collected (or printed) in an array of size $n = n_b n_s$. After collecting the data, the deviation is calculated using Eq. (3.6), changing the block size n_b from 2 to some value (maximally allowed is $N/2$), as well as n_s, to keep the product to be the number of data $n = n_b n_s$. Case $n_b = 2$ ($n_b = N/2$) corresponds to large (small) groups of data. Finally, from the graph $(\sigma(n_b), n_b)$ the optimal value of n is determined to be the point there σ reaches the plateu. The error cannot depend on the size of each block n_b, so the value of σ is constant for $n_b > n_{optimal}$. The behaviour of (σ_{n_b}, n_b) is presented in Fig. 3.1. For small number of data, like in Fig. (3.1), the error estimate is not a smooth function of n_s.
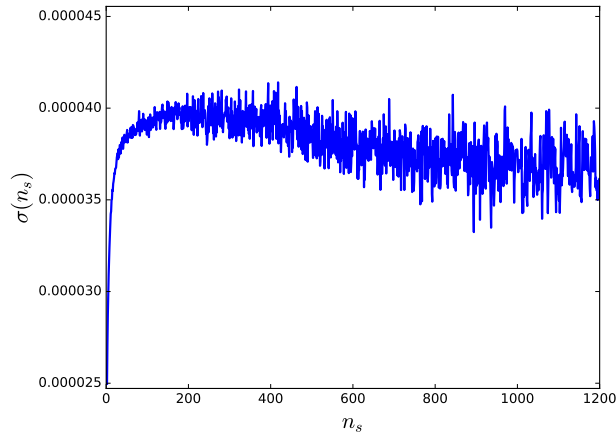
Figure 3.1: Dependence of error estimation of energy with the size of each data block for the 10 particles in an isotropic harmonic trap interacting with the scattering length $a = 10^{-1}a_{ho}$, obtained with VMC. Number of MC steps is $200,000$ and the number of walkers is 100.

3.3 Variational Monte Carlo

Variational Monte Carlo is a variational stochastic method used to approximate the ground state properties. Variational formulation of the Schrödinger equation (2.1) is given by equation

$$\delta E[\psi] = 0 \tag{3.7}$$

where $E[\psi]$ is given by

$$E[\psi] = \frac{\int \psi^* \hat{H}\psi \, d\boldsymbol{R}}{\int \psi^* \psi \, d\boldsymbol{R}} \tag{3.8}$$

Wave function ψ can be written as

$$\psi = \sum_{n=0}^{\infty} c_n \phi_n \tag{3.9}$$

where c_n are scalar coeficients and ϕ_n is the n-th eigenstate of time independent Schrödinger equation

$$H\phi_n = E_n\phi_n \tag{3.10}$$

With the normalization condition

$$\sum_i |c_i|^2 = 1 \qquad (3.11)$$

Variational method gives upper bound to exact energy E_0 , since from eq. 3.7 and eq. 3.9 we have

$$\int \psi^* H \psi \, d\mathbf{R} = \sum_n |c_n|^2 E_n = E_0 + \sum_{n=1}^{\infty} |c_n|^2 E_n \geq E_0 \qquad (3.12)$$

In a VMC method one writes a trial ground state wavefunction, calculates its expectation value of energy using Metropolis algorithm for different variational parameters, and those parameters that minimise the energy define our best guess of the true ground state. For a given trial wavefunction $\psi_T(\boldsymbol{\alpha}, \mathbf{R})$, where $\boldsymbol{\alpha} = (\alpha_1, \alpha_2, \ldots, \alpha_p)$ is a set of p numbers that parameterise ψ_T, the energy of the ground state for a given $\psi_T(\boldsymbol{\alpha}, \mathbf{R})$ is given by

$$E(\boldsymbol{\alpha}) = \frac{\int \psi_T^*(\boldsymbol{\alpha}, \mathbf{R}) H \psi_T(\boldsymbol{\alpha}, \mathbf{R}) \, d\mathbf{R}}{\int \psi_T^*(\boldsymbol{\alpha}, \mathbf{R}) \psi_T(\boldsymbol{\alpha}, \mathbf{R}) \, d\mathbf{R}} \qquad (3.13)$$

The global minimum of $E(\boldsymbol{\alpha})$ implicitly determines $\psi_T(\boldsymbol{\alpha}, \mathbf{R})$ via parameters $\boldsymbol{\alpha}$. Calculation of integral in eq. (3.13) can be rewritten in a form compatible with the Metropolis algorithm

$$E(\boldsymbol{\alpha}) = \int E_L(\boldsymbol{\alpha}, \mathbf{R}) \rho(\boldsymbol{\alpha}, \mathbf{R}) \, d\mathbf{R} \qquad (3.14)$$

where

$$E_L(\boldsymbol{\alpha}, \mathbf{R}) = \frac{H\psi(\boldsymbol{\alpha}, \mathbf{R})}{\psi(\boldsymbol{\alpha}, \mathbf{R})} \qquad (3.15)$$

$$\rho(\boldsymbol{\alpha}, \mathbf{R}) = \frac{|\psi(\boldsymbol{\alpha}, \mathbf{R})|^2}{\int d\mathbf{R} \psi_T^*(\boldsymbol{\alpha}, \mathbf{R}) \psi_T(\boldsymbol{\alpha}, \mathbf{R})} \qquad (3.16)$$

More generally, the expectation value of some operator O can be written as

$$O(\boldsymbol{\alpha}) = \int O_L \rho(\boldsymbol{\alpha}, \mathbf{R}) \, d\mathbf{R} \qquad (3.17)$$

where

$$O_L = \frac{O\psi_T(\boldsymbol{\alpha}, \mathbf{R})}{\psi_T(\boldsymbol{\alpha}, \mathbf{R})} \qquad (3.18)$$

Monte Carlo integration of eq. (3.14) is carried out numerically using Metropolis algorithm(sec. 3.1). There are two key parts of the VMC method. First, one equilibrates the system by moving the walkers using Metropolis algorithm a large number of steps to make sure we sample the correct $\rho(\alpha, \boldsymbol{R})$. Second, walkers are moved and energy is sampled for every step. In both parts, the crucial step is updating the optimal step length to make sure system goes optimally fast through the phase space. Additionaly, for large systems it is desirable that Metropolis algorithm is changed in the following way. Instead of moving one walker, which is a set of positions of particles $\boldsymbol{r}_1, \boldsymbol{r}_2, \ldots, \boldsymbol{r}_n$, particles are moved one by one. Moving particles as a configuration "freezes" each walker much more often than moving each particle one by one. However, we still have correlations between steps, and the method of blocking is used for evaluation of standard deviation.

Finally, the VMC code needs to be iterated over different values of $\boldsymbol{\alpha}$ to obtain optimal parameters. Pseudocode for VMC algorithm is in Alg. 1. Usual dependence of estimators with the number of Monte Carlo steps in the VMC integration is shown in Fig. 3.2. First part of this MC simulation (first $\approx 2,000$ MC steps) is interpreted as the equilibration of distribution function which we want to sample, and is omitted when calculating the estimate value.
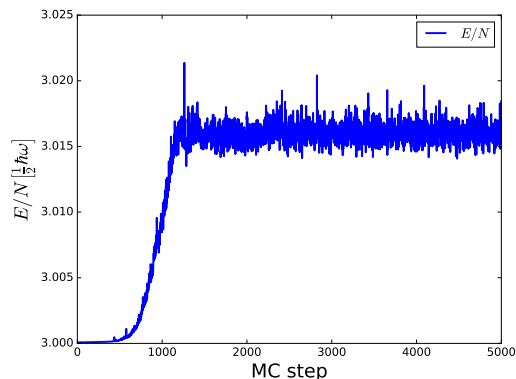

Figure 3.2: Dependence of energy estimator with the size of each data block for 3 particles in an isotropic harmonic trap interacting with the scattering length $a = 10^{-2}a_{ho}$, obtained with VMC. The number of walkers is 100.

Algorithm 1 VMC Pseudocode

    Initialization of coordinates for every walker and every particle
    for loop over steps **do**
        for loop over walkers **do**
            for loop over particles **do**
                $\boldsymbol{r}_{i;new} = \boldsymbol{r}_{i;old} + step \times \Delta \boldsymbol{R}$
                $T = \rho(\boldsymbol{\alpha}, \boldsymbol{R}_{new})/\rho(\boldsymbol{\alpha}, \boldsymbol{R}_{old})$
                if $T > 1$ **then**
                    Accept step
                if $T < 1$ **then**
                    Generate random number r in the interval $[0 : 1]$
                    if $r < T$ **then**
                        Accept step
        Save $E_L(\boldsymbol{R}, \alpha)$
        if acceptance rate < wanted acceptance rate **then**
            step = step * 0.95
        else
            step = step * 1.05

3.4 Diffusion Monte Carlo

Diffusion Monte Carlo [13] is a stochastic method of solving the imaginary-time Schrödinger equation exactly, for a given potential surface. The distribution function we are sampling in the Diffusion Monte Carlo (DMC) method is

$$f(\boldsymbol{R}, t) = \phi(\boldsymbol{R}, t)\psi_T(\boldsymbol{R}) \tag{3.19}$$

where $\psi_T(\boldsymbol{R})$ is the optimized trial wavefunction, our best guess for the ground state wavefunction. Function $\phi(\boldsymbol{R}, t)$ is the exact wavefunction of the system at time t, which can be written as

$$\phi(\boldsymbol{R}, t) = \sum_n c_n e^{-i(E_n - E_0)t/\hbar}\phi_n(\boldsymbol{R}) \tag{3.20}$$

where $\phi_n(\boldsymbol{R})$ is time-independent n-th eigenstate of the Hamiltonian. Rewriting the Eq. (3.20) in imaginary time $t = i\tau$, we see that $\phi(\boldsymbol{R}, \tau)$ decays to the ground state wavefunction $\phi_0(\boldsymbol{R})$ in the $\tau \to \infty$ limit. This is the main idea of DMC; to sample f from Eq. (3.19) in the $t \to \infty$ limit to obtain the

ground state properties of the system. Since only ground state is considered, this method is exact only for zero temperature. Complete formalism of DMC method is made in imaginary time, so we will denote t to be imaginary time from now on. Applying the Hamilton operator to Eq. (3.19) we get the (imaginary) time dependent equation of $f(\boldsymbol{R}, t)$

$$-\frac{\partial f}{\partial t} = -\frac{\hbar^2}{2m}\nabla^2_{\boldsymbol{R}}f + \frac{\hbar^2}{2m}\nabla \cdot (\boldsymbol{F}f) + (E_L(\boldsymbol{R}) - E)\,f \qquad (3.21)$$

where $\boldsymbol{F}$ is called the quantum force, E_L is the local energy

$$\boldsymbol{F}(\boldsymbol{R}) = 2\frac{\nabla\psi_T}{\psi_T} \qquad (3.22)$$

$$E_L = \frac{\hat{H}\psi_T}{\psi_T} \qquad (3.23)$$

The Eq. (3.21) is of the form

$$-\frac{\partial f}{\partial t} = \hat{O}f = \left(\hat{O}_1 + \hat{O}_2 + \hat{O}_3\right)f \qquad (3.24)$$

where operators $\hat{O}_i$ on the right hand side of Eq. (3.21) are associated with diffusion, continuity and decay processes, respectively. Eq. (3.21) is solved iteratively using the Green function formalism

$$f(\boldsymbol{R}', t + \Delta t) = \int d\boldsymbol{R}\, G(\boldsymbol{R}', \boldsymbol{R}, \Delta t)f(\boldsymbol{R}, t) \qquad (3.25)$$

where

$$G(\boldsymbol{R}', \boldsymbol{R}, \Delta t) = \langle \boldsymbol{R}'| \exp(-\hat{O}\Delta t)\,|\boldsymbol{R}\rangle \qquad (3.26)$$

It is not possible to find Green function defined in Eq. (3.26) exactly, since the operators $\hat{O}_i$ do not commute with each other. But the Green function for each term can be solved independently, so what is usually done are approximations with respect to the powers of Δt, such as

$$e^{-\hat{O}\Delta t} = e^{-\hat{O}_3\Delta t/2}e^{-\hat{O}_2\Delta t/2}e^{-\hat{O}_1\Delta t/2}e^{-\hat{O}_1\Delta t/2}e^{-\hat{O}_2\Delta t/2}e^{-\hat{O}_3\Delta t/2} + \mathcal{O}(\Delta t^3) \quad (3.27)$$

From Eq. (3.27) we see that

$$\langle \boldsymbol{R}'| e^{-\hat{O}\Delta t/2}\,|\boldsymbol{R}\rangle = \int d\boldsymbol{R}'\, d\boldsymbol{R}''\, d\boldsymbol{R}'''G_3\left(\boldsymbol{R}', \boldsymbol{R}'', \frac{\Delta t}{2}\right)$$

$$\times G_2\left(\boldsymbol{R}'', \boldsymbol{R}''', \frac{\Delta t}{2}\right)G_1\left(\boldsymbol{R}''', \boldsymbol{R}, \frac{\Delta t}{2}\right) \qquad (3.28)$$

where

$$G_3\left(\boldsymbol{R}', \boldsymbol{R}'', \frac{\Delta t}{2}\right) = \langle \boldsymbol{R}'| e^{-\hat{O}_3 \frac{\Delta t}{2}} |\boldsymbol{R}''\rangle \qquad (3.29)$$

$$G_2\left(\boldsymbol{R}'', \boldsymbol{R}''', \frac{\Delta t}{2}\right) = \langle \boldsymbol{R}''| e^{-\hat{O}_2 \frac{\Delta t}{2}} |\boldsymbol{R}'''\rangle \qquad (3.30)$$

$$G_1\left(\boldsymbol{R}''', \boldsymbol{R}, \frac{\Delta t}{2}\right) = \langle \boldsymbol{R}'''| e^{-\hat{O}_1 \frac{\Delta t}{2}} |\boldsymbol{R}\rangle \qquad (3.31)$$

Analytical solutions to the Green functions (3.29)-(3.31) are given by [13]

$$G_1(\boldsymbol{R}', \boldsymbol{R}, t) = \left(2\pi\hbar^2 t/m\right)^{-3N/2} \exp\left[-\frac{(\boldsymbol{R}' - \boldsymbol{R})^2}{2\hbar t/m}\right] \qquad (3.32)$$

$$G_2(\boldsymbol{R}', \boldsymbol{R}, t) = \delta\left(\boldsymbol{R}' - \boldsymbol{R}(t)\right) \text{ where } \begin{cases} \boldsymbol{R}(0) = \boldsymbol{R} \\ \frac{d\boldsymbol{R}}{dt} = \frac{\hbar^2}{2m}\boldsymbol{F} \end{cases} \qquad (3.33)$$

$$G_3(\boldsymbol{R}', \boldsymbol{R}, t) = \exp\left[-\left(E_L(\boldsymbol{R}) - E\right)\right] \delta(\boldsymbol{R}' - \boldsymbol{R}) \qquad (3.34)$$

We see that the evolution of f in time Δt can be approximated by three consecutive operations: gaussian movement, move due to the quantum drift force, and branching factor. One MC step of DMC method, for a given walker, is summarized below.

1. Gaussian displacement $\boldsymbol{R}_1 = \boldsymbol{R} + \boldsymbol{\chi}$, where $\boldsymbol{\chi}$ is vector drawn from gaussian distribution $\exp\left(-\chi^2/(2\Delta t\hbar^2/m)\right)$. This is numerically implemented using *gasdev* number generator with the spread $\sqrt{\hbar^2\Delta t/m}$

2. Calculate quantum force $\boldsymbol{F}_1(\boldsymbol{R}_1)$

3. First step: $\boldsymbol{R}_2 = \boldsymbol{R}_1 + \frac{1}{2}\frac{\hbar^2}{2m}\Delta t\boldsymbol{F}_1$

4. Calculate quantum force $\boldsymbol{F}_2(\boldsymbol{R}_2)$

5. Second step: $\boldsymbol{R}_2 = \boldsymbol{R}_1 + \frac{1}{2}\frac{\hbar^2}{2m}\Delta t\frac{\boldsymbol{F}_1 + \boldsymbol{F}_2}{2}$

6. Calculation of local energy $E_L(\boldsymbol{R}_2)$, quantum force $\boldsymbol{F}(\boldsymbol{R}_2)$ and other properties

7. Final step: $\boldsymbol{R}' = \boldsymbol{R}_1 + \frac{\hbar^2}{2m}\Delta t\boldsymbol{F}$

8. For each walker calculate weight as $w = \exp\left[-\Delta t\left(0.5(E_L(\boldsymbol{R}_2) + E_L(\boldsymbol{R})) - E_{\text{ref}}\right)\right]$ and replicate it $\text{int}\left[w + ran()\right]$ times, where $ran()$ is random number drawn from uniform distribution in interval $[0:1]$

3.4.1 Pure estimators

Estimators sampled by the DMC method are called the *mixed* estimators since the probability distribution function we sample is $f = \phi_0 \psi_T$. Therefore we have a potential bias due to the trial wavefunction. For operators that commute with the Hamiltonian, sampling the PDF f gives the same results as it would if we sampled ϕ_0^2. However, for operators that do not commute with the Hamiltonian, we need to treat the trial wavefunction bias carefully in order to obtain exact results, and this is usually done with the *pure* estimators. Algorithm for pure estimators can be found in [9] [10], and our tests of numerical implementation are presented in Fig. 4.3 and 5.1

Chapter 4

Bose mixture with repulsive interactions

In this chapter the Monte Carlo study of two-component bosonic mixture with repulsive interspecies and intraspecies interactions in a harmonic trap at zero temperature is presented. Two-body repulsive interaction is modeled as hard-sphere potential (Eq. 2.31)

$$V_{int}(r) = \begin{cases} \infty & r < a_{ij} \\ 0 & r > a_{ij} \end{cases} \tag{4.1}$$

Repulsive interactions produce positive scattering lengths: $a_{11}, a_{22}, a_{12} > 0$. The Hamiltonian is given by

$$\hat{H} = -\sum_i^{N_1+N_2} \frac{\hbar^2}{2m_i}\nabla_i^2 + \sum_{i<j}^{N_1+N_2} V_{int}(r_{ij}) + \sum_i^{N_1+N_2} \frac{1}{2}m_i\omega^2 r_i^2 \tag{4.2}$$

where N_i is number of particles of species i, m_i is mass of species i particle. The trial wavefunction we use is constructed as product of two-body and one-body solutions

$$\psi_T(\boldsymbol{R}) = \prod_{i<j}^{N_1} f_{11}(r_{ij}) \prod_{i<j}^{N_2} f_{22}(r_{ij}) \prod_{i,j}^{N_1,N_2} f_{12}(r_{ij}) \prod_i^{N_1+N_2} \phi(\boldsymbol{r}_i) \tag{4.3}$$

where the two-body term is

$$f_{ij}(r) = \begin{cases} 0 & r < a_{ij} \\ 1 - \frac{a_{ij}}{r} & r > a_{ij} \end{cases} \tag{4.4}$$

26

and one-body term due to harmonic confinement is

$$\phi(\boldsymbol{r}_i) = \exp(-\alpha_i r_i^2) \tag{4.5}$$

Trial wavefunction (4.3) has only two variational parameters: α_1 and α_2, and their values for the single-body problem are

$$\alpha_i = \frac{1}{2a_{ho,i}^2} \tag{4.6}$$

where the $a_{ho,i}$ is length unit associated with the confinement

$$a_{ho,i} = \sqrt{\frac{\hbar}{m_i \omega}} \tag{4.7}$$

where ω is characteristic harmonic frequency of the trapping potential. Trial wavefunction does not have a variational parameter for the repulsive two-body interaction. It is shown in Sec. 4.2 and 4.3 that even this trial wavefunction can give very accurate description of the system at the VMC level.

4.1 Test run of the code: one particle in isotropic harmonic trap

To see if our implementation is correct, we will make a test run for a system where all the properties are known exactly: single particle in an isotropic harmonic trap. Ground state energy and wavefunction are given by [21]

$$E_0 = \frac{3}{2}\hbar\omega \tag{4.8}$$

$$\psi_0 = \left(\frac{m\omega}{\hbar\pi}\right)^{3/4} \exp\left(-\frac{m\omega r^2}{2\hbar}\right) \tag{4.9}$$

We can use the exact wavefunction to be the trial wavefunction for the input in the DMC code, but with different value of the variational parameter from the exact one to check whether our code is sensitive to the choice of the input trial wavefunction. We will use the trial wavefunction of the form

$$\psi_0 = \exp(-\alpha r^2/2) \tag{4.10}$$

where we take α to be the variational parameter. The exact value of α is

$$\alpha_{LHO} = \frac{m\omega}{2\hbar} \qquad (4.11)$$

If Fig. 4.1 we plotted energy versus Δt for $\alpha = 0.5\alpha_{LHO}$. At the VMC level, energy is $E = 3.74(8)\frac{\hbar\omega}{2}$. Even tough we use quadratic DMC algorithm, timestep analysis shows linear dependence of energy versus timestep. However, we see correct extrapolation of energy to $\Delta t = 0$. In Fig. 4.2 we plotted kinetic energy, potential energy and the number of walkers versus the timestep of the simulations, where we see that kinetic and potential energy are not fluctuating about the exact value since the DMC code samples mixed estimators. On Fig. 4.3 we plotted single particle density profile in an isotropic trap for different values of initial variational parameters, to test the implementation of pure estimator algorithm. Finally, in Table 4.1 we give energies of two particle system in harmonic trap for two different values of scattering length, which are in agreement with those reported in [6].
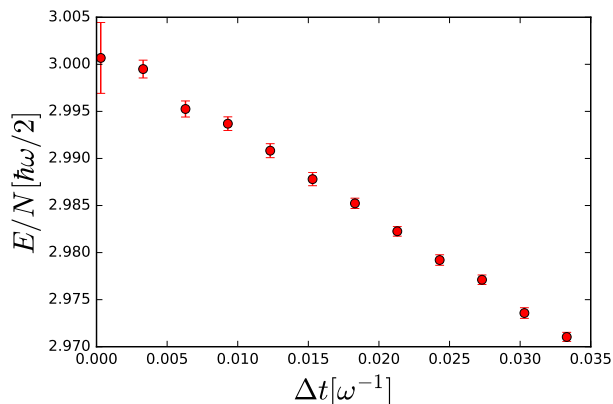
Figure 4.1: Dependence of the single particle energy in a harmonic trap on imaginary timestep Δt, for the trial wavefunction (Eq. 4.3), with a variational parameter set far from exact value: $\alpha = 0.5\alpha_{LHO}$. Number of MC steps is 200000. Extrapolation of the linear fit to $\Delta t = 0$ predicts $3.001(7)\frac{\hbar\omega}{2}$.

(a) $\alpha = 0.5\alpha_{LHO}$
                                               (b) $\alpha = 0.5\alpha_{LHO}$
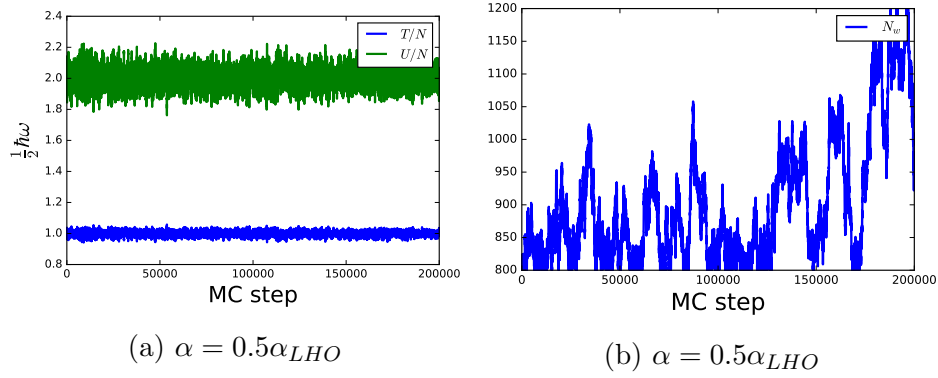
Figure 4.2: Evolution of the number of walkers N_w, kinetic and potential energy with the simulation timestep. Imaginary timestep used is $\Delta t = 3 \times 10^{-3}$.
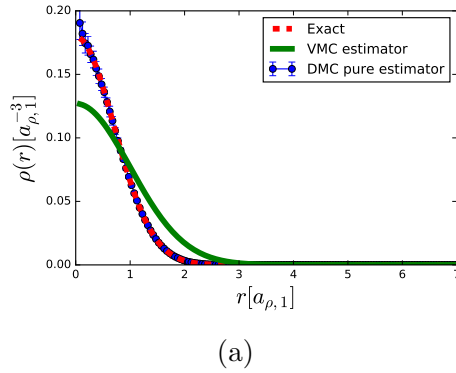

(a)

Figure 4.3: Density profile of a single particle in isotropic trap predicted by VMC and DMC for the wavefunction parameter $\alpha = 0.5\alpha_{LHO}$. Number of steps per block in pure estimator algorithm is 5000, and imaginary timestep used is $\Delta t = 3 \times 10^{-3}\omega^{-1}$.

29

Table 4.1: Comparison of results from our code with those reported in [6] for a two-particle system in a harmonic trap. Imaginary timestep used is $\Delta t = 1.5 \times 10^{-4} \omega^{-1}$.

$a\,[a_{ho,1}]$	Our DMC code	Results from [6]
0.00433	$3.00346(3)\hbar\omega$	$3.00346(1)\hbar\omega$
0.433	$3.38(1)\hbar\omega$	$3.3831(7)\hbar\omega$

4.2   Single component analysis

In this section the results for the single component weakly repulsive Bose gas in a harmonic trap are presented. Usual description of such systems is based on the Gross-Pitaevski equation, which can be written in nondimensional form, rescaling the lengths with the harmonic length a_{ho} and energies with $\hbar^2/(2ma_{ho}^2)$

$$\left(-\widetilde{\nabla}^2 + \widetilde{r}^2 + 8\pi \frac{Na}{a_{ho}}\widetilde{\phi}^2(\widetilde{\boldsymbol{r}})\right)\widetilde{\phi}(\widetilde{\boldsymbol{r}}) = 2\widetilde{\mu}\widetilde{\phi}(\widetilde{\boldsymbol{r}}) \qquad (4.12)$$

We see that the system properties in the mean-field regime are completely determined by the factor Na/a_{ho}. It is shown in [14] that such description is valid in the limit $N \to \infty$ and $a \to 0$, keeping the Na/a_{ho} constant. Physical interpretation of this parameter is the importance of interaction in the system, since $E_{int}/E_{kin} \sim Na/a_{ho}$ [15].

First we compare the results obtained using our trial wave function (Eq. 5.4) with the DMC calculations from [6], summarized in Table 4.2. Variational parameters are set to ideal one. We see that even without varying the parameters there is a great overlap between input trial wavefunction and the exact one.

Table 4.2: Comparison of VMC and DMC energies of a single component system, for $a = 0.433a_{ho}$. Variational parameters used are exact one: $\alpha = 1/(2a_{ho}^2)$.

N	$E_{VMC}\,[\hbar\omega]$	$E_{DMC}\,[\hbar\omega]$
3	5.59(8)	5.553(3)
5	10.693(5)	10.577(2)
10	26.478(5)	26.22(8)
20	67.36(1)	66.9(4)

We have two universalities in our physics: the Gross-Pitaevski universality valid in the limit $(N \rightarrow \infty, a \rightarrow 0)$ for a given Na/a_{ho}, and the "real" universality, where we describe physics with only one parameter: the scattering length a, that includes beyond mean field effects. Therefore, the Gross-Pitaevski equation is valid only for very dilute systems.

We search for the range of validity of the Gross-Pitaevski universality by calculating the DMC energies as a function of Gross-Pitaevski parameter Na/a_{ho} in Fig. (4.4). Since the results for different number of particles do not fall on a single curve, as predicted by the Gross-Pitaevski equation, we conclude that our calculations are picking up fluctuations not included in the mean-field physics. Our DMC results show that Gross-Pitaevski universality is recovered only for small values of Na/a_{ho}, but as we increase the interaction strength we see that energy starts to depend separately on N and a. It is also interesting to note there is a convergence toward a single curve as we increase the number of particles. We do not have the Gross-Pitaevski numerical solver to compare the results, but we get the same qualitative results like in the literature, [19], [6].

Another important question to solve is for which values of parameters we have universal physics, such that the interaction is described solely by the scattering length a. This was analyzed in [6] for the types of systems we focus on, and the author claims that the universal description is valid for approximately $n(0)a^3 \leq 2 \cdot 10^{-3}$, where ρ is density at the center of mass. In Fig. 4.6 we see the effect of repulsive interactions on the overall density profile is to reduce the central density and make the system more flat. Increasing the interaction we approach the Thomas-Fermi limit, valid in for $Na/a_{ho} \gg 1$ and $N \gg 1$, where the system can be well approximated to be locally homogenous.

In Fig. 4.6 we calculate the dependence of gas parameter $n(0)a^3$ on Na/a_{ho}, and see that the universality breaks sooner for smaller systems, where we follow the rule that the universality is recovered only for $n(0)a^3 < 2 \times 10^{-3}$ [6]. Our interest is to investigate strongly interacting systems for which the Gross-Pitaevski parameter is big, and we see that for 100 particles (and above) we can use the scattering length as the only parameter of the interaction for Gross-Pitaevski parameter up to 10.
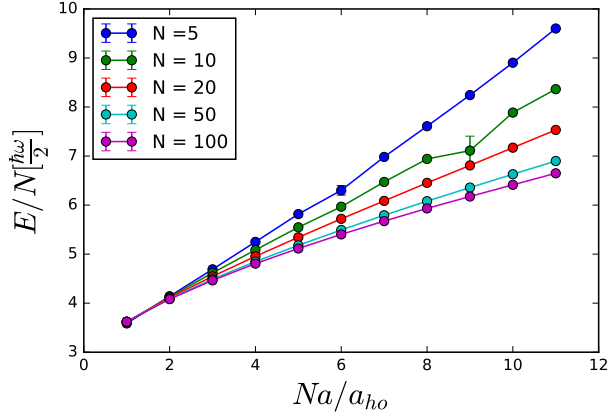
Figure 4.4: Dependence of E_{DMC}/N with the Gross-Pitaevski universal parameter Na/a_{ho}. The mean-field breakdown, resulting from the fact that the energy does not depend solely on GP parameter for a fixed value of Na/a_{ho}, is occuring sooner for smaller systems with big scattering lengths.
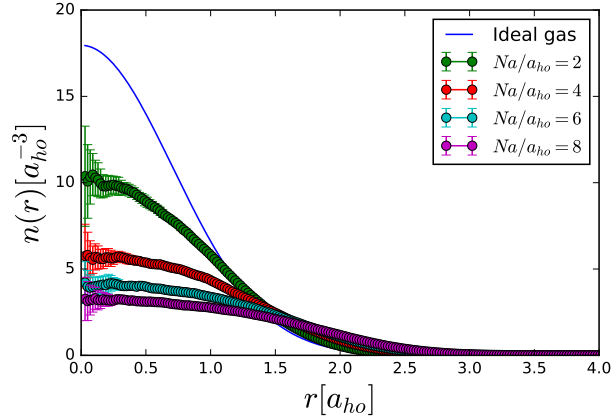

Figure 4.5: Density profiles for different interactions obtained using pure estimators for a system of 100 particles. Lowering of the density, called the quantum depletion, happens due to the repulsive interactions.
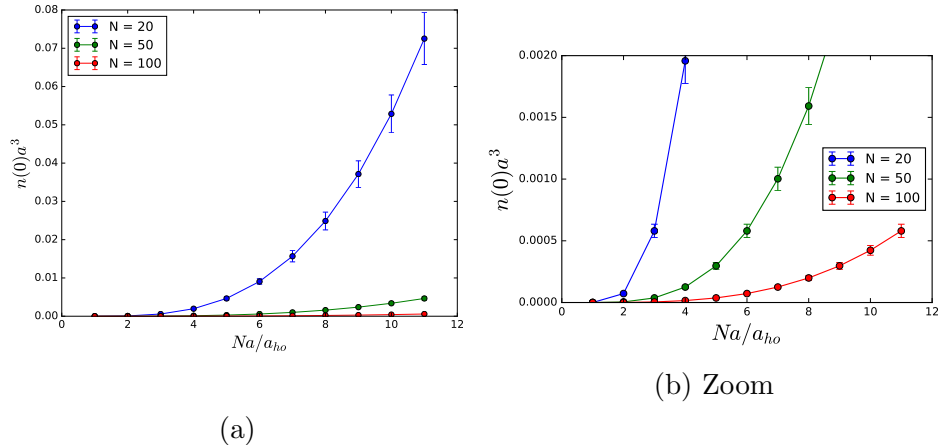
Figure 4.6: Dependence of diluteness parameter $n(0)a^3$ with the Gross-Pitaevski parameter Na/a_{ho}, where we see that the universality breaks down sooner for smaller systems.

4.3 Phase diagram of two-component mixture

In this section the QMC study of repulsive Bose-Bose mixture is presented. Usually, system properties of ultracold systems are obtained by solving the Gross-Pitaevski equation (2.43), which is a mean-field approximation. From the mean-field point of view the properties of the bosonic mixture are characterised by the coupling constants $g_{ij} = 2\pi\hbar^2 a_{ij}/m_{ij}$, where a_{ij} is interaction between species i and j, and $m_{ij} = m_i m_j/(m_i + m_j)$ is reduced mass of two-particle system with mass m_i and m_j. Miscibility of the system in the mean-field approximation for a homogenous system is determined by the relationship of g_{12}, g_{11} and g_{22}. For $g_{12}^2 < g_{11}g_{22}$ the condensates overlap in space, while for $g_{12}^2 > g_{11}g_{22}$ they phase-separate. In this section, we will test the applicability of this miscibility criterion for the strongly interacting small systems in the harmonic trap, and present what are the beyond mean field effects on the system properties.

There is no universal parametar determining the properties of two-component systems from the mean-field perspective, like we had in a single component one. Additionally, there is no diluteness parameter from which we can determine the validity of constructing potentials knowing only scattering length. So we focus only on those coupling constants (g_{11}, g_{22}, g_{12}) that slightly devi-

ate from the single component values that have universal interaction. In other words, we will use $m_2 \sim m_1$, $a_{12} \sim a_{11} \sim a_{22}$. We define the phase diagram as in [12], where the system states are defined with $(g_{12}/g_{22}, g_{11}/g_{12}, N_1, N_2)$, because the authors find that for trapped gases the location of the phase boundary between mixed and separated states depends also on the particle number. This is where we make comparisson with the mean-field, since in the paper [12] the structural properties of two-component Bose systems in harmonic trap are determined with Gross-Pitaevski equation, and the authors claim that this is a good way of characterizing the system. Our results suggest that we should use additional parameters, to account the effects of mass disbalance and the effect of interaction strength, for the systems containing at most 100 particles. Results that back up this indication are presented in subsection 4.3.2.

4.3.1 Same scattering lengths, different mass

We first present the results for the system with and $a_{11} = a_{22} = a_{12}$. Different mass ratios are used: $m_2 = m_1$, $m_2 = 1.5m_1$, $m_2 = 4m_1$. Parameters for the optimized trial wavefunction, VMC and DMC energies are shown in Tables (4.3-4.5). We see that the VMC and DMC energies are very close, so we conclude that there is great overlap between the trial wavefunction and the exact ground state wavefunction. The dependence of energy on different mass ratios can be qualitatively understood by the fact that the repulsion drives the lighter particles toward energetically higher single-particle states [20]. In the ideal case the lighter particles are more delocalized in a trap, so the repulsive interspecies interaction can push them to the edge of the drop more easily. This can be seen on Fig. (4.7,4.8), where partial densities from the center of mass are plotted. For large enough scattering lengths the separation occurs, and this separation is more pronounced for bigger differences between m_2 and m_1.

Table 4.3: Optimal variational parameters, VMC and DMC energies for $a_{11} = a_{22} = a_{12} = a$, $m_2 = m_1$, where $a_{ho,i} = \sqrt{\hbar/(m_i\omega)}$. The number of particles is 100.

Na/a_{ho}	$\alpha_1 \left[1/a_{ho,1}^2\right]$	$\alpha_2 \left[1/a_{ho,2}^2\right]$	$E_{VMC}/N \left[\frac{1}{2}\hbar\omega\right]$	$E_{DMC}/N \left[\frac{1}{2}\hbar\omega\right]$
2	0.48	0.47	4.0820(1)	4.0810(1)
8	0.52	0.51	5.939(1)	5.929(3)
14	0.55	0.56	7.322(5)	7.30(5)

Table 4.4: Optimal variational parameters, VMC and DMC energies for $a_{11} = a_{22} = a_{12} = a$, $m_2 = 1.5m_1$, where $a_{ho,i} = \sqrt{\hbar/(m_i\omega)}$. The number of particles is $50 + 50$.

Na/a_{ho}	$\alpha_1 \left[1/a_{ho,1}^2\right]$	$\alpha_2 \left[1/a_{ho,2}^2\right]$	$E_{VMC}/N \left[\frac{1}{2}\hbar\omega\right]$	$E_{DMC}/N \left[\frac{1}{2}\hbar\omega\right]$
2	0.48	0.49	4.157(4)	4.157(0)
8	0.516	0.552	6.085(1)	6.083(7)
14	0.541	0.567	7.507(9)	7.506(2)

Table 4.5: Optimal variational parameters, VMC and DMC energies for $a_{11} = a_{22} = a_{12} = a$, $m_2 = 4m_1$, where $a_{ho,i} = \sqrt{\hbar/(m_i\omega)}$. The number of particles is $50 + 50$.

Na/a_{ho}	$\alpha_1 \left[1/a_{ho,1}^2\right]$	$\alpha_2 \left[1/a_{ho,2}^2\right]$	$E_{VMC}/N \left[\frac{1}{2}\hbar\omega\right]$	$E_{DMC}/N \left[\frac{1}{2}\hbar\omega\right]$
2	0.48	0.49	4.290(4)	4.287(5)
8	0.60	0.58	6.308(2)	6.28(7)
14	0.67	0.56	7.837(9)	7.83(3)

(a) $Na/a_{ho} = 2$ (b) $Na/a_{ho} = 8$ (c) $Na/a_{ho} = 14$
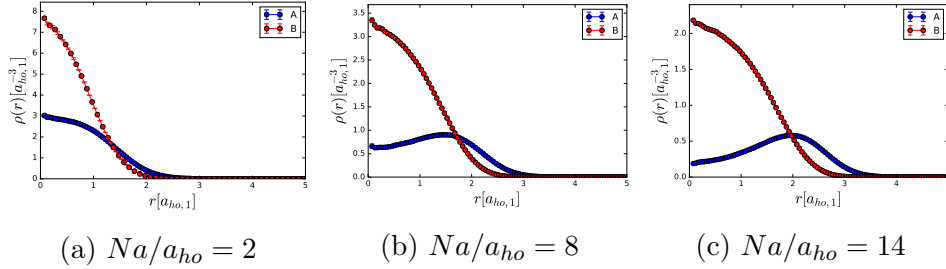
Figure 4.7: Evolution of density profiles with the increase of interaction $a_{11} = a_{22} = a_{12} = a$. Mass ratio is $m_2/m_1 = 1.5$. Number of particles $N_1 = N_2 = 50$.
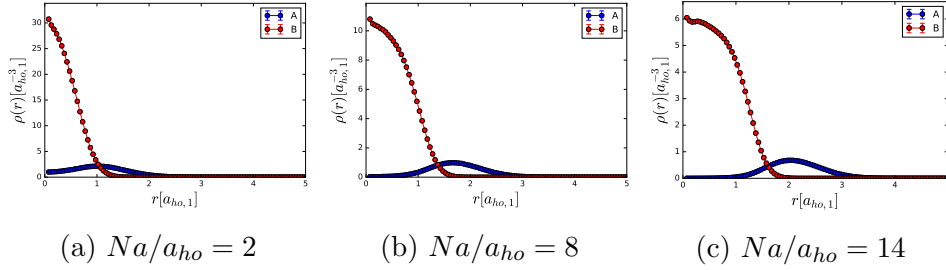

(a) $Na/a_{ho} = 2$ (b) $Na/a_{ho} = 8$ (c) $Na/a_{ho} = 14$

Figure 4.8: Evolution of density profiles with the increase of interaction $a_{11} = a_{22} = a_{12} = a$. Mass ratio is $m_2/m_1 = 4$. Number of particles $N_1 = N_2 = 50$.

4.3.2   Different phases of two-component Bose system

In this subsection we want to test the predictions from [12], where the authors claim the phase diagram can be spanned, for a given N_1 and N_2, with g_{12}/g_{22} and g_{11}/g_{12} only. We focus on the parameters given in Table 4.6, which are about the same points that have been used in [12], where all the results are obtained by solving the Gross-Pitaevski equations. The points are also graphically represented in Fig. 4.9. Here we use the full power of quantum Monte Carlo to exactly solve the many-body Schroedinger equation and predict the properties exactly.

Table 4.6: Phase space points on which we focus on. Mean field prediction for homogeneous systems is based on the relative strenghts of coupling constants; we have separation for $g_{12}^2 > g_{11}g_{22}$, mixing for $g_{12}^2 < g_{11}g_{22}$, critical point for $g_{12}^2 = g_{11}g_{22}$.

Label	g_{12}/g_{22}	g_{11}/g_{12}	Mean field prediction
a	3.0	0.33	Separation
b	0.75	0.75	Critical point
c	0.75	1.7	Mixing
d	1.2	1.7	Mixing
e	1.7	1.7	Critical point
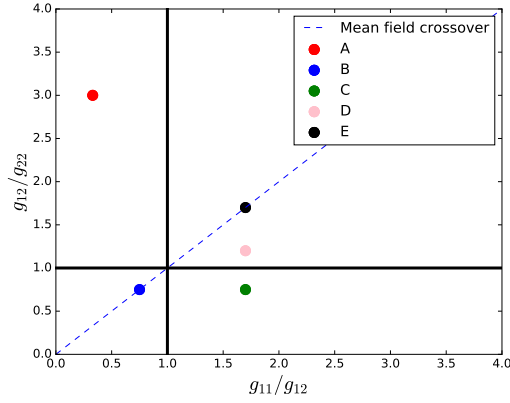
Figure 4.9: Graphical representation of the phase space points from Table 4.6. Mean field theory for homogeneous system predicts separation (mixing) for all the points above (below) the mean field crossover (dashed line).

From the mean field point of view, the structural properties do not depend separately on mass and scattering length, but only through the combination defined by the coupling constants $g_{ij} = 2\pi\hbar^2 a_{ij}/m_{ij}$. In the subsections 4.3.2-4.3.2 we present density profiles obtained with the DMC mixed estimator algorithm, changing the interaction from weakly to strongly interacting, to present how the interaction strength changes the profile of the system. We plotted mixed estimators since they have much smaller noise than the pure estimators, and we justify this supstitution because of the small difference between VMC and DMC energies, meaning that the trial wavefunction greatly overlaps the exact wavefunction.

Generally we find that mean field separation criteria $g_{12}^2 > g_{11}g_{22}$ for homogeneous is not applicable any more. This was also observed in [12]. Since this system is not homogeneous, but trap favours overlap in numerical studies mentioned in [12], three different types of density profiles were indentified. The phase is considered mixed when both components overlap at the trap centre. In a symmetrical demixed phase one component forms a shell structure around the other. In an asymmetrical demixed phase the centers of mass of the two components do not coincide.

The authors have thus identified a new characterization of the mixture, by the difference in the normalized trap-centre density

$$\Delta n_{norm} = \frac{n_{c,1}(0)}{\max n_{c,1}(\boldsymbol{r})} - \frac{n_{c,2}(0)}{\max n_{c,2}(\boldsymbol{r})} \qquad (4.13)$$

When two components overlap strongly than Δn_{norm} is zero, and when they are in a strongly demixed phase where one pushes the other from the centre Δn_{norm} is either 1 or -1. In the following we will compare our results both with the mean field criterion for the homogeneous systems and the predictions of [12].

For the weakly interacting trapped system $(Na_{11}/a_{ho,1} = 2)$, for all the points in the phase diagram except those in Fig. 4.20, we have partially mixed phase, contrary to the mean field predictions and the predictions by [12]. This property can be explained by the fact that for the weak interparticle interaction, the harmonic trap plays a major role in structural properties. As we increase the interaction strength, all the clouds become more delocalized, and the density profiles start to form different shapes. Separation types for the strongly interacting system $Na_{11}/a_{ho,1} = 14$ are summarized in Table 4.7.

Table 4.7: Summary of the structural properties of the strongly interacting systems for which $Na_{11}/a_{ho,1} = 14$.

Points 4.6		Our results	Mean field prediction
A	$m_B = m_A$	Asym. phase	
	$m_B = 1.5m_A$	Symm. demixed	Separation
	$m_B = 4m_A$	Symm. demixed	
B	$m_B = m_A$	Mixed	
	$m_B = 1.5m_A$	Mixed	Critical point
	$m_B = 4m_A$	Mixed	
C	$m_B = m_A$	Mixed	
	$m_B = 1.5m_A$	Mixed	Mixing
	$m_B = 4m_A$	Mixed	
D	$m_B = m_A$	Mixed	
	$m_B = 1.5m_A$	Mixed	Mixing
	$m_B = 4m_A$	Symm. demixed	
E	$m_B = m_A$	Mixed	
	$m_B = 1.5m_A$	Symm. demixed	Critical point
	$m_B = 4m_A$	Symm. demixed	

In most points of the phase diagram we do not have a unique way of defining whether the specied are mixed or separated since there is relatively large overlap between two species even in the strongly interacting regime. This is probably because the harmonic trap still plays major role in stabilizing the system. Density profiles for the same coupling constant fractions from Table (4.6), but with different mass ratios show different behaviour. We observe that with the large difference in mass we don't need to have strong interaction to separate the species.

In point A (4.6) we have an agreement with [12] only for $m_B = m_A$ case, but a bad agreement for $m_B \neq m_A$. We obtain partial mixing for $m_B = 1.5m_A$, and fully symmetrically demixed phase for $m_B = 4m_A$.

In point B (4.6) we have qualitatively same density profiles for $m_B = m_A$ and $m_B = 1.5m_A$ with the results from [12]. We have not obtained the full separation of species as in [12] but rather the partial mixing, indicating the stabilizing role of the harmonic trap. For the $m_B = 4m_A$ case we obtain a strong shell-like structure of species B, a completely different profile from the one we get with the other mass ratios. We suspect this is a result of relatively

strong interaction between species B, compared with the other interaction strengths.

In point C (4.6) we obtain qualitatively the same results as [12] only for $m_B = m_A$. The species mix almost completely for $m_B = m_A$, but as we increase the mass ratio m_B/m_A the species A goes more toward the edge of the trap.

In point D and E (4.6) we see very similar profiles as in [12]. Species partially mix, with the species A more delocalized.
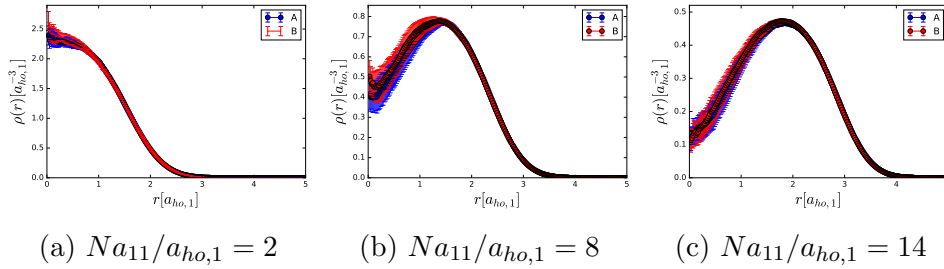
Density profiles for $m_2 = m_1$

(a) $Na_{11}/a_{ho,1} = 2$ (b) $Na_{11}/a_{ho,1} = 8$ (c) $Na_{11}/a_{ho,1} = 14$

Figure 4.10: Point A from Table 4.6 for $m_2 = m_1$. Mean field prediction: separation.

(a) $Na_{11}/a_{ho,1} = 2$ (b) $Na_{11}/a_{ho,1} = 8$ (c) $Na_{11}/a_{ho,1} = 14$
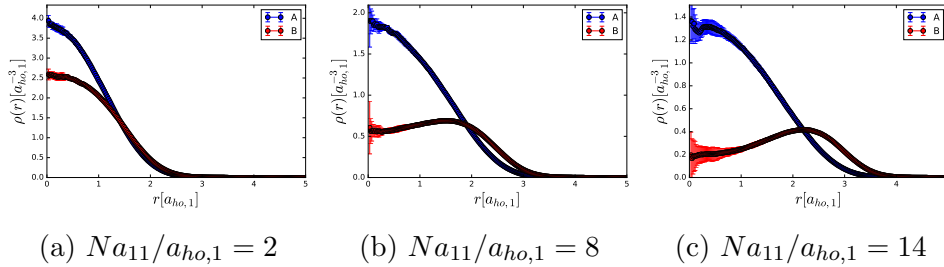
Figure 4.11: Point B from Table 4.6 for $m_2 = m_1$. Mean field prediction: critical point.

(a) $Na_{11}/a_{ho,1} = 2$ (b) $Na_{11}/a_{ho,1} = 8$ (c) $Na_{11}/a_{ho,1} = 14$
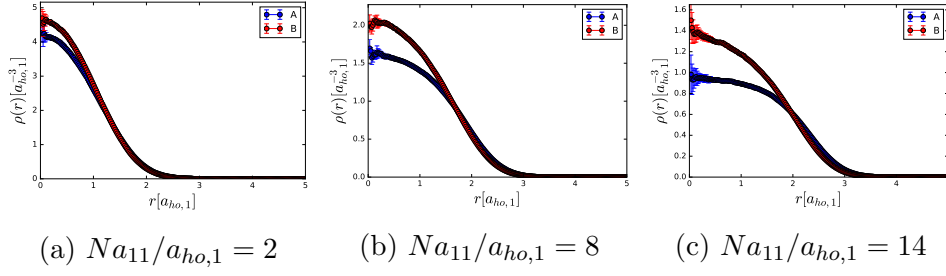
Figure 4.12: Point C from Table 4.6 for $m_2 = m_1$. Mean field prediction: mixing.

(a) $Na_{11}/a_{ho,1} = 2$ (b) $Na_{11}/a_{ho,1} = 8$ (c) $Na_{11}/a_{ho,1} = 14$
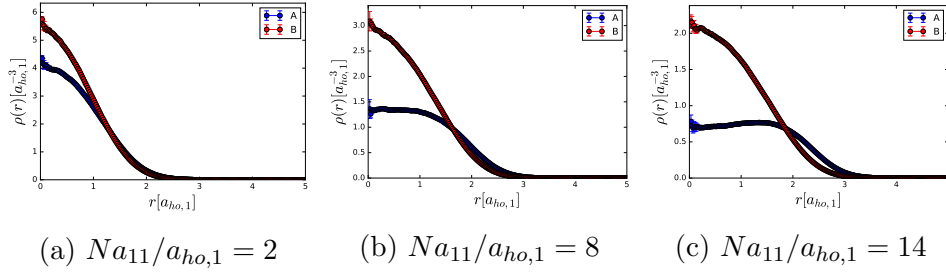
Figure 4.13: Point D from Table 4.6 for $m_2 = m_1$. Mean field prediction: mixing.

(a) $Na_{11}/a_{ho,1} = 2$ (b) $Na_{11}/a_{ho,1} = 8$ (c) $Na_{11}/a_{ho,1} = 14$
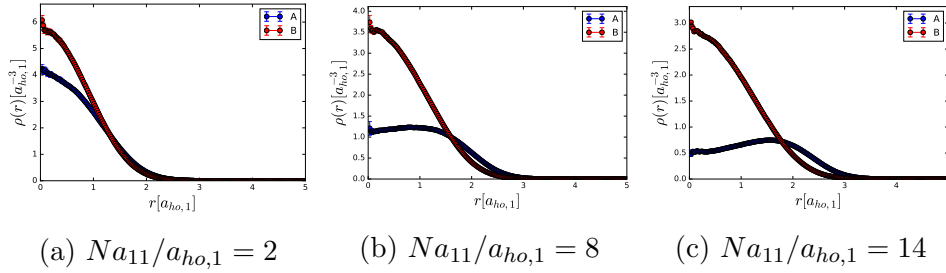
Figure 4.14: Point E from Table 4.6 for $m_2 = m_1$. Mean field prediction: critical point.

Density profiles for $m_2 = 1.5m_1$

(a) $Na_{11}/a_{ho,1} = 2$ (b) $Na_{11}/a_{ho,1} = 8$ (c) $Na_{11}/a_{ho,1} = 14$
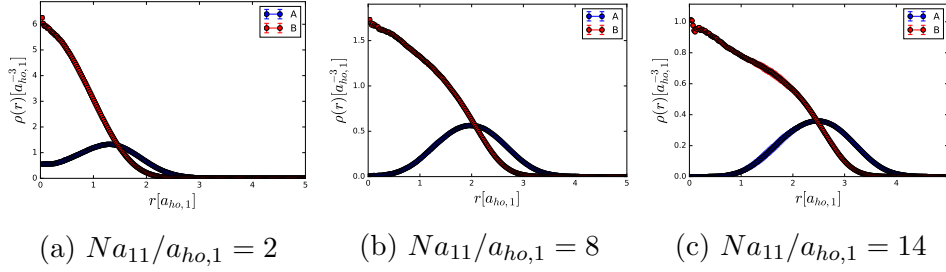
Figure 4.15: Point A from Table 4.6 for $m_2 = 1.5m_1$. Mean field prediction: separation.

(a) $Na_{11}/a_{ho,1} = 2$ (b) $Na_{11}/a_{ho,1} = 8$ (c) $Na_{11}/a_{ho,1} = 14$
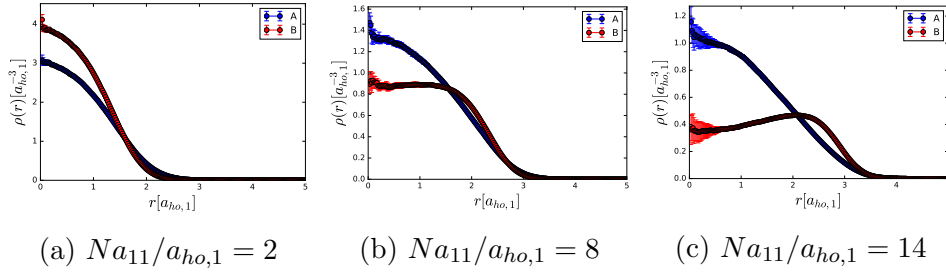
Figure 4.16: Point B from Table 4.6 for $m_2 = 1.5m_1$. Mean field prediction: critical point.

(a) $Na_{11}/a_{ho,1} = 2$ (b) $Na_{11}/a_{ho,1} = 8$ (c) $Na_{11}/a_{ho,1} = 14$
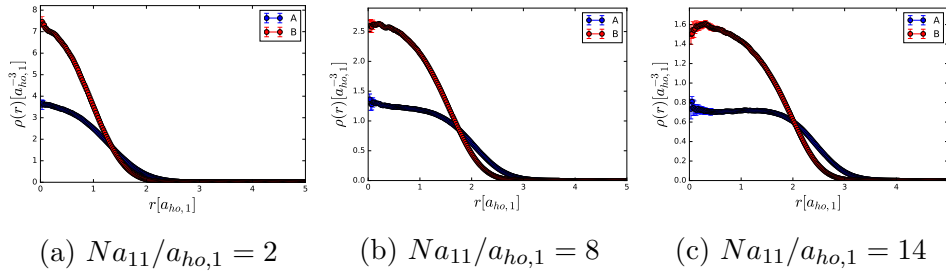
Figure 4.17: Point C from Table 4.6 for $m_2 = 1.5m_1$. Mean field prediction: mixing.

(a) $Na_{11}/a_{ho,1} = 2$ (b) $Na_{11}/a_{ho,1} = 8$ (c) $Na_{11}/a_{ho,1} = 14$
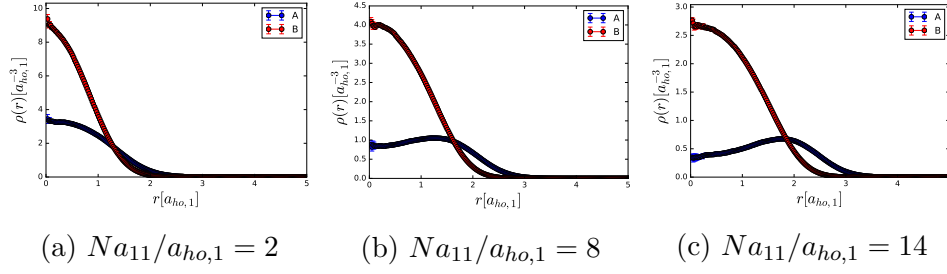
Figure 4.18: Point D from Table 4.6 for $m_2 = 1.5m_1$. Mean field prediction: mixing.

(a) $Na_{11}/a_{ho,1} = 2$ (b) $Na_{11}/a_{ho,1} = 8$ (c) $Na_{11}/a_{ho,1} = 14$
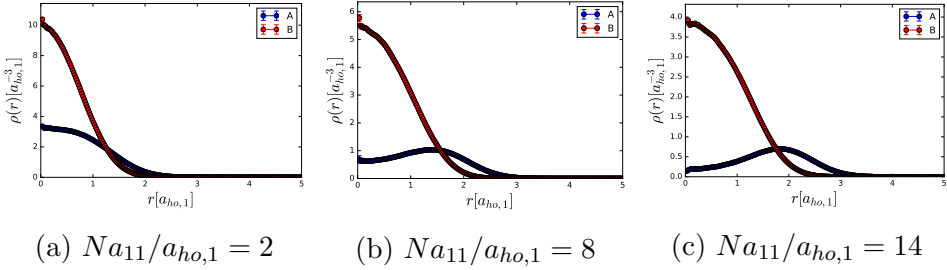
Figure 4.19: Point E from Table 4.6 for $m_2 = 1.5m_1$. Mean field prediction: critical point.

Density profiles for $m_2 = 4m_1$

(a) $Na_{11}/a_{ho,1} = 2$ (b) $Na_{11}/a_{ho,1} = 8$ (c) $Na_{11}/a_{ho,1} = 14$
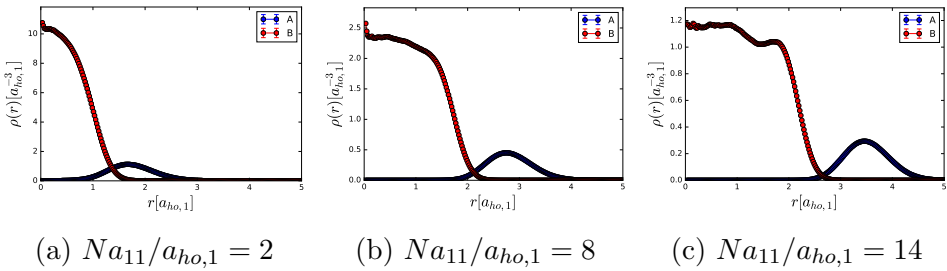
Figure 4.20: Point A from Table 4.6 for $m_2 = 4m_1$. Mean field prediction: separation.

(a) $Na_{11}/a_{ho,1} = 2$ (b) $Na_{11}/a_{ho,1} = 8$ (c) $Na_{11}/a_{ho,1} = 14$
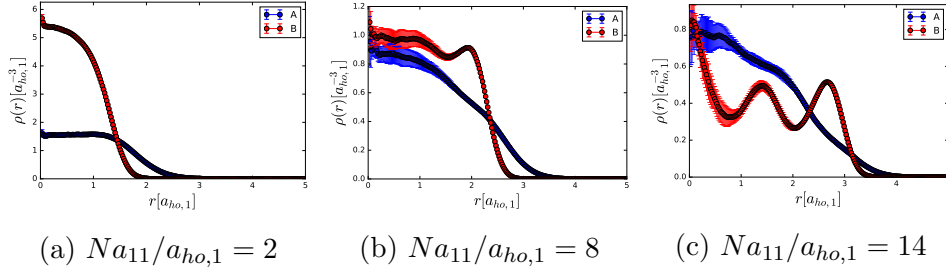
Figure 4.21: Point B from Table 4.6 for $m_2 = 4m_1$. Mean field prediction: critical point.

(a) $Na_{11}/a_{ho,1} = 2$ (b) $Na_{11}/a_{ho,1} = 8$ (c) $Na_{11}/a_{ho,1} = 14$
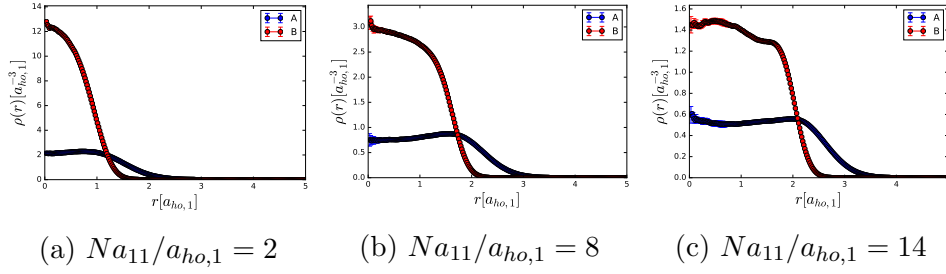
Figure 4.22: Point C from Table 4.6 for $m_2 = 4m_1$. Mean field prediction: mixing.

(a) $Na_{11}/a_{ho,1} = 2$ (b) $Na_{11}/a_{ho,1} = 8$ (c) $Na_{11}/a_{ho,1} = 14$
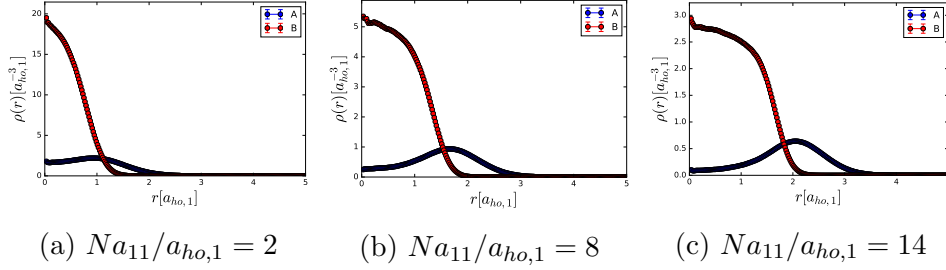
Figure 4.23: Point D from Table 4.6 for $m_2 = 4m_1$. Mean field prediction: mixing.

44

(a) $Na_{11}/a_{ho,1} = 2$ (b) $Na_{11}/a_{ho,1} = 8$ (c) $Na_{11}/a_{ho,1} = 14$
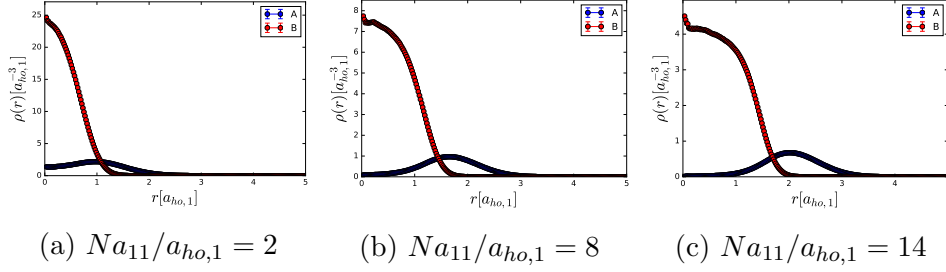
Figure 4.24: Point E from Table 4.6 for $m_2 = 4m_1$. Mean field prediction: critical point.

4.4   Summary

In this chapter we analyzed both single-component and two-component Bose gases in harmonic confinement. We tested the implementation of VMC and DMC codes, found the range of universality for the systems containing 100 particles at most for the single component system, and analyzed the phase diagram of two-component system. We obtain qualitative agreement of our results with one obtained in the mean field approximation [12] in some points of the phase diagram, but the deviations in other. We suspect that the more general description of two-component Bose gases in a harmonic trap should incorporate mass difference and interaction strength, on top of the way the phase diagram is spanned in [12].

Chapter 5

Bose mixture with the repulsive intraspecies and attractive interspecies interaction

In this chapter the Monte Carlo study of two-component bosonic mixture with repulsive intraspecies and attractive intraspecies interactions in vacuum is presented. In the low-density regime, we describe the interaction between particles by one parameter: the scattering length a which is positive (negative) for repulsive (attractive) interactions. Since this is the only parameter describing the system, we can choose the forms of the potential to be as simple as possible: hard-core potential for the repulsive, and square well potential for the attractive interactions. Relation between scattering lengths and all the details of interaction for such potentials are given in subsections 2.2.1 and 2.2.2. The Hamiltoian of the system is

$$H = -\sum_{i}^{N} \frac{\hbar^2 \nabla_i^2}{2m_i} + \sum_{i<j}^{N} V_{ij}(r_{ij}) \tag{5.1}$$

where for $i = 1, 2$

$$V_{ii} = \begin{cases} \infty & r < a_{ii} \\ 0 & r > a_{ii} \end{cases} \tag{5.2}$$

$$V_{12} = \begin{cases} -V_0 & r < R_0 \\ 0 & r > R_0 \end{cases} \tag{5.3}$$

We choose trial wavefunction of the system to be

$$\psi_T(\boldsymbol{R}) = \prod_{i<j}^{N_1} f_{11}(r_{ij}) \prod_{i<j}^{N_2} f_{22}(r_{ij}) \prod_{i,j}^{N_1,N_2} f_{12}(r_{ij}) \tag{5.4}$$

where for $i = 1, 2$

$$f_{ii}(r) = \begin{cases} 0 & r < a_{ii} \\ 1 - \frac{a_{ii}}{r} & r > a_{ii} \end{cases} \tag{5.5}$$

$$f_{12}(r) = \begin{cases} \frac{\sin(kr)}{r} & r < L \\ \exp\left[\frac{k(r-L)}{\tan(kL)}\right] \frac{\sin(kL)}{r} & r > L \end{cases} \tag{5.6}$$

Variational parameters of the problem are only k and L.

5.1 Test run of the code: two particles interacting with square well potential

To check the implementation of attractive two-particle square well interaction, we will compare the results of our code with the system that is analitically solvable: dimer of two spinless particles. The square well is characterized by the potential depth V_0 and the range R. The wavefunction of bound system is given by [22]

$$f_{12}(r) = \begin{cases} A\frac{\sin(kr)}{r} & r < R \\ B\frac{\exp(-k_2 r)}{r} & r > R \end{cases} \tag{5.7}$$

where r is separation between particles, $\mu = m_1 m_2/(m_1 + m_2)$ is reduced mass of the system, A and B are normalization constant which are mutually dependent because of continuity conditions, and k_1 and k_2 are given by

$$k_1 = \sqrt{\frac{2\mu(V_0 + E)}{\hbar^2}} \tag{5.8}$$

$$k_2 = \sqrt{-\frac{2\mu E}{\hbar^2}} \tag{5.9}$$

There is at least one bound state for the potential depths above V_{min} [21] given by

$$V_{min} = \frac{\pi^2 \hbar^2}{8\mu R^2} \tag{5.10}$$

47

Relation between energy and the parameters of interaction is obtained from the continuity requirements, and is given by

$$\sqrt{\frac{2\mu}{\hbar^2}(V_0 + R)} \cot\left[\sqrt{R\frac{2\mu}{\hbar^2}(V_0 + E)}\right] = -\sqrt{-\frac{2\mu E}{\hbar^2}} \qquad (5.11)$$

We check our code by setting $R = 10a_{11}$, and changing V_0 in the range where two particles have only one bound state. Lengths are scaled with the scattering lengths asociated with intraspecies interaction. Parameters of the trial wavefunction are set deliberately wrong: $L = 14a_{11}$ and $k = 0.6\pi/L$. In Fig. 5.1 we compare predictions of VMC and DMC methods with the exact ones. DMC gives results in excelent agreement with the exact ones.
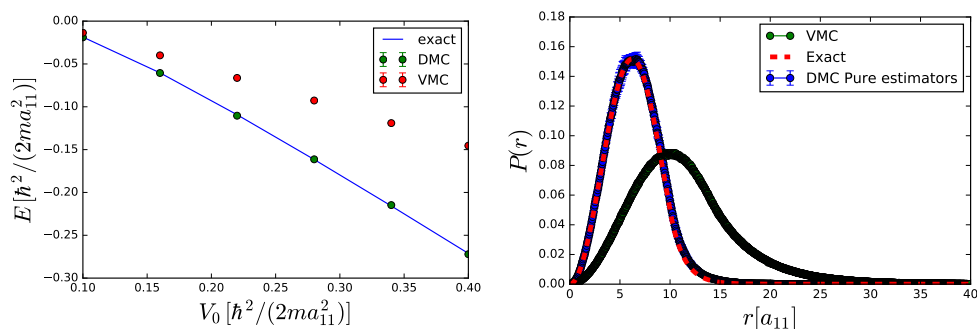
Figure 5.1: Check of our DMC code for $R = 10a_{11}$.

5.2 Test run of the code: deeply bound $5 + 5$ system

To make further test of the code, we calculate energy of the deeply bound $5 + 5$ system, with the parameters of attractive interaction set to $R = 5a_{11}$ and $V_0 = \hbar^2/(2ma_{11}^2)$. Optimal variational parameters and minimum VMC energy are presented in Table 5.1, with energies obtained using wavefunction parameters other than the optimal ones. We test whether the DMC energies give the same value for different input parameters. Results show a bias because of the trial wavefunction, which can be removed by introducing larger number of walkers. This property is presented in Fig. 5.2, where we make timestep analysis for different number of walkers, and for different

wavefunction parameters. We have not obtained convergence with respect to the number of walkers due to the strong bias of the wavefunction other than the optimized one because we were limited by numerical requirements at the time. The convergence of DMC energy for the optimized trial wavefunction is obtained however. This is because the overlap between the true ground state and the optimized trial wavefunction is great. Large overlap is also reflected in the very small difference between mixed and pure estimators of density profile of species A, shown in Fig. 5.3 , whereas we see big difference when we use other input parameters. In Fig. 5.3 can also be seen the comparison of noise between mixed and pure estimators. Comparison of density profiles obtained with pure estimators for different trial wavefunction is shown in Fig. 5.4, where we see that the pure estimator is insensitive to the choice trial wavefunction, within the statistical uncertainty.

Table 5.1: Variational MC energies for different values of input parameters. Parameters of interaction are $R = 5a_{11}$, $V_0 = \hbar^2/(2ma_{11}^2)$.
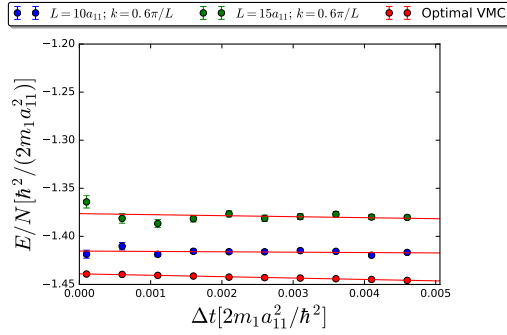
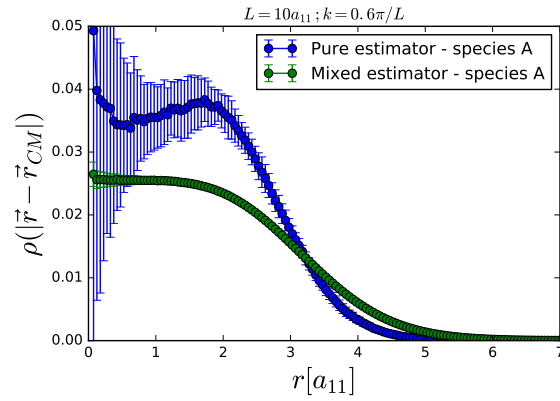| Wavefunction parameters	$E_{VMC}/N\,[\hbar^2/(2ma_{11}^2)]$
$L = 10a_{11}$; $k = 0.6\pi/L\,a_{11}^{-1}$	$-0.593(2)$
$L = 15a_{11}$; $k = 0.6\pi/L\,a_{11}^{-1}$	$-0.242(8)$
$L = 5.66a_{11}$; $k = 0.37a_{11}^{-1}$ (Optimal VMC)	$-1.417(8)$
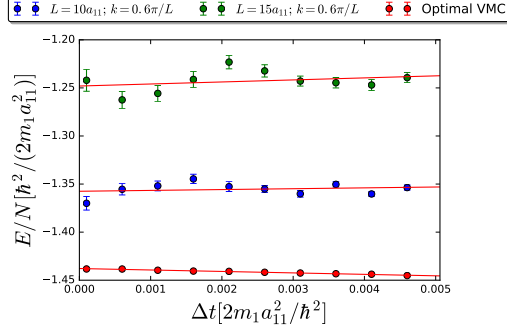
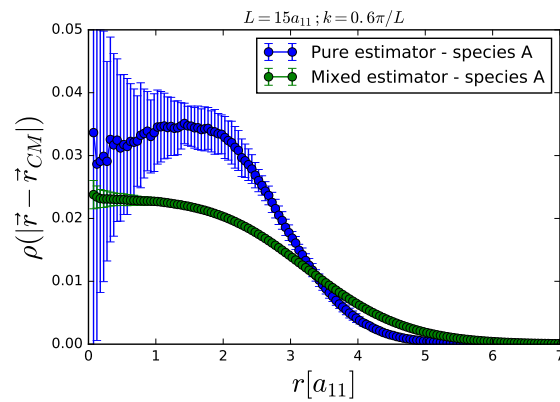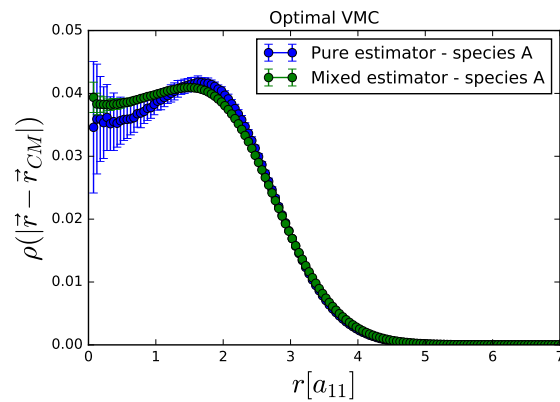(a) $N_w = 100$
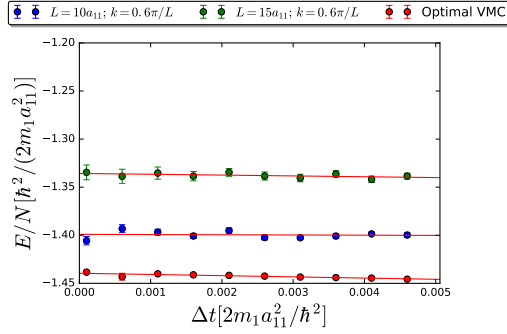
(b) $N_w = 250$

(c) $N_w = 500$

Figure 5.2: Timestep analysis for different number of walkers, and for different input trial wavefunction parameters. The wavefunction bias is gradually removed by introducing larger number of walkers.

(a)

(b)

(c)

Figure 5.3: Comparison of mixed and pure estimators of density profile of species A from the center-of-mass. Species B has the same profile. Number of walkers used is 500, and the number of steps per block used is 10000 for and pure estimators.
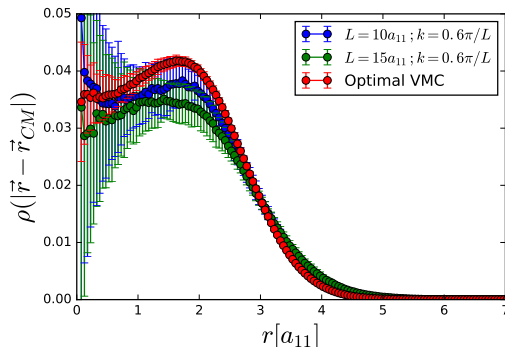
Figure 5.4: Comparison of density profiles of species A obtained using pure estimator algorithm. Number of walkers is 500, number of steps per block is 10000.

## 5.3 Properties of the weakly bound droplet

Droplet formation in systems with repulsive intraspecies and attractive interspecies is predicted by [7], where the author claims that the mean-field collapse in the regime $g_{12}^2 > g_{11}g_{22}$ is stabilized by quantum fluctuations, resulting in a very dilute droplet. In this section we will present properties of the symmetric systems: $m_2 = m_1$, $a_{11} = a_{22}$, $N_1 = N_2$, in the regime where the mean-field predicts collapse. First we will search the critical value of g_{12} for which the droplet forms, and then calculate the central density of the drop in order to validate the low-density regime of the stabilization phenomena and to predict the density of the homogeneous system. All the calculations are made by means of VMC and DMC methods.

5.3.1 VMC analysis

Trial wavefunction used is in a form (5.4), where the two-particle correlations are described by (5.5) and (5.6). We scan a_{12} line, varying the parameters for each a_{12}, to give the prediction of a_{12}^{crit} on a VMC level. In Fig. 5.5 minimum VMC energies vs. a_{12} are plotted, for different number of particles and for different square-well ranges. It is expected that in the low-density regime the energy depends on the scattering length solely, which is not obtained on the VMC level. Therefore we cannot exactly predict the critical value of a_{12} with the current trial wavefunction. However we see the trend of increasing a_{12}^{crit}

by increasing the number of particles. In Table 5.2 we write lower bound estimations of critical a_{12} values with respect to the number of particles. We see that the droplet formation in our case happens for different interaction strengths than discussed in [7], where the stabilization is predicted to happen at $g_{12} \approx \sqrt{g_{11}g_{22}}$. There are two sources of dicrepancy between our results and predictions from [7]: VMC calculations are model-dependent, and our droplets have too few particles. Therefore our future predictions will be based on the DMC calculations with large number of particles, which is outside the scope of this thesis. Finally, we plot partial density of the droplet for different number of particles in Fig. 5.6, for the scattering lengths in Table 5.2. Droplet grows in size while with N, but interestingly the saturation is not obtained even for the $100 + 100$ system. However, this can also be a result of a trial wavefuncion bias.
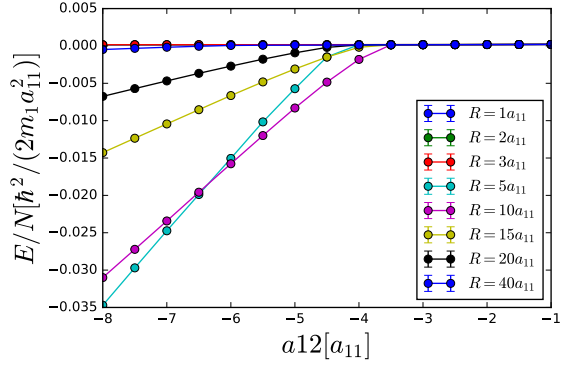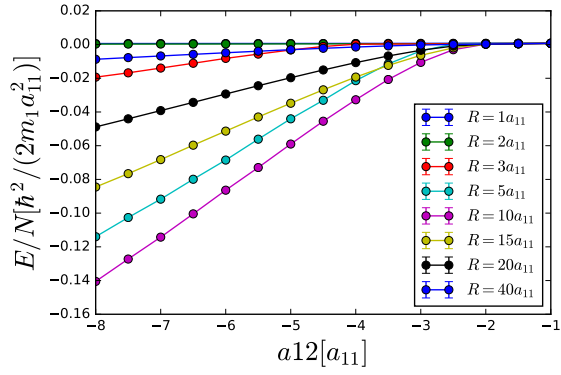
(a) $N = 25 + 25$
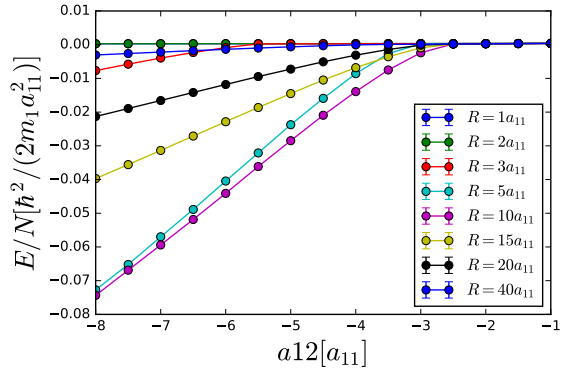
(b) $N = 50 + 50$

(c) $N = 100 + 100$

Figure 5.5: Dependence of energy vs. a_{12} scattering lengths for different number of particles.

Table 5.2: Lower bound of critical values of scattering lengths on the VMC level for different number of particles. Values used are obtained for square-wells ranges $R_0 = 10a_{11}$.

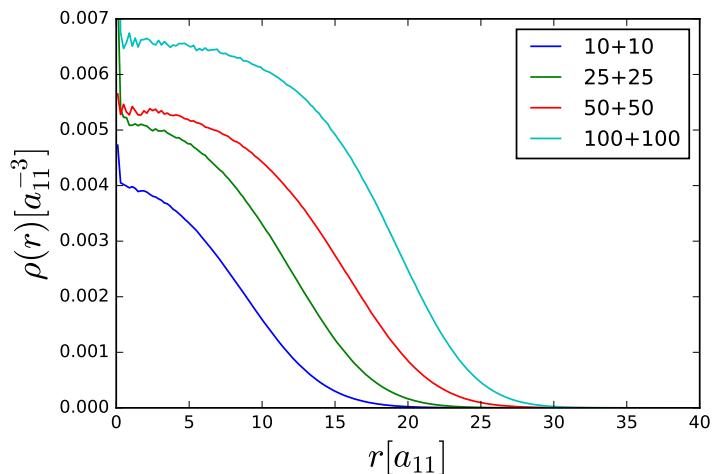| N	$a_{12}^{crit} [a_{11}]$
$10 + 10$	-7.5
$25 + 25$	-4
$50 + 50$	-3
$100 + 100$	-2.5

Figure 5.6: VMC density profiles for a_{12} from Table 5.2.

5.4 Summary

In this chapter, the study of two-component Bose mixture with attractive interspecies and repulsive intraspecies interactions is presented, on a variational level. We made sure the code is implemented correctly, and presented crude estimations of critical values of a_{12} for which the droplet appears. Calculations on a variational lever show dependence on another parameter besides the scattering length, which could be a result of a trial wavefunction model, or an effect due to finite number of particles. In future, the exact DMC calculations for large number of particles will be performed in order to reach final conclusions about the system properties.

Bibliography

[1] Gerald D. Mahan: *Many-Particle Physics*, Kluwer Academics/Plenum Publichers, Third Edition (2000)

[2] Anderson, M. H., J. R. Ensher, M. R. Matthews, C. E. Wieman, and E. A. Cornell, 1995, Science 269, 198.

[3] Immanuel Bloch, Jean Dalibard, and Wilhelm Zwerger, Rev. Mod. Phys. 80, 885 – Published 18 July 2008

[4] Lev Pitaevski, Sandro Stringari, *Bose-Einstein Condensation*, Oxford University Press, 2003

[5] S. Giorgini, J. Boronat, J. Casulleras, *Ground state of a homogeneous Bose gas: A diffusion Monte Carlo calculation*, Phys. Rev. A, 60, 6 (1999)

[6] D. Blume, Chris H. Greene: *Quantum corrections to the ground state energy of a trapped Bose-Einstein condensate: A diffusion Monte Carlo calculation*, http://arxiv.org/abs/cond-mat/0009220

[7] D. S. Petrov: *Quantum Mechanical Stabilization of a Collapsing Bose-Bose Mixture*, Phys. Rev. Lett. 115, 155302 (2015)

[8] D. S. Petrov, G. E. Astrakharchik: *Ultradilute low-dimensional liquids*, Phys. Rev. Lett. 117, 100401 (2016)

[9] A. Sarsa, J. Boronat, J. Casulleras: *Quadratic diffusion Monte Carlo and pure estimators for atoms*, J. Chem. Phys. 116, 5956 (2002)

[10] K. S. Liu, M. H. Kalos, and G. V. Chester, *Quantum hard spheres in a channel*, Phys. Rev. A 10, 303 (1974).

[11] Siu A. Chin: *Quadratic diffusion Monte Carlo algorithms for solving atomic many-body problems*, Phy. Rev. A 42 (1990)

[12] Kean Loon Lee, Nils B. Jørgensen, I-Kang Liu, Lars Wacker, Jan J. Arlt, Nick P. Proukakis: *Phase Separation and Dynamics of two-component Bose-Einstein condensates*, Phys. Rev. A 94, 013602 (2016)

[13] J. Boronat 'Monte Carlo simulations at zero temperature: Helium in one, two and three dimensions', Series on Advances in Quantum Many-Body Theory-Vol. 4, *Microscopic approaches to quantum liquids in confined geometries*, Chapter 2 (World Scientific 2004)

[14] E.H. Lieb and J. Yngvason, *Bosons in a trap: A rigorous derivation of the Gross-Pitaevskii energy functional*, Phys. Rev. A 61, 043602-1–13 (2000).

[15] F. Dalfovo, S. Giorgini, L. P. Pitaevskii and S. Stringari: *Theory of Bose-Einstein condensation in trapped gases*, Rev. Mod. Phys. 71, 463 (1999).

[16] N. N. Bogoliubov, *On the theory of superfluidity*, J. Phys. U.S.S.R. 11, 23 1947.

[17] T. D. Lee, K. Huang, and C. N. Yang, *Eigenvalues and Eigenfunctions of a Bose System of Hard Spheres and Its Low-Temperature Properties*, Phys. Rev. 106, 1135 1957.

[18] T. T. Wu, *Ground State of a Bose System of Hard Spheres*, Phys. Rev. 115, 1390 1959.

[19] J. L. DuBois and H. R. Glyde, *Bose-Einstein condensation in trapped bosons: A variational Monte Carlo analysis*, Phys. Rev. A 63, 023602 – Published 5 January 2001

[20] Hong Ma, Tao Pang: *Path-integral quantum Monte Carlo study of a mixture of Bose–Einstein condensates*, Physics Letters A 351 (2006) 92–96

[21] Nouredine Zettili, *Quantum Mechanics: Concepts and Applications*, Wiley; 2nd edition (February 24, 2009)

[22] H.T.C Stoof, K.B. Gubbels, D.B.M. Dickerscheid, *Ultracold quantum fields*, Springer; 1st edition (2009)

[23] E. Timmermans, P. Tommasini, K. Huang: *Variational Thomas-Fermi theory of a nonuniform Bose condensate at zero temperature*, Phys. Rev. A 55 (1997)